PRODUCTION AND CHARACTERIZATION OF ACTIVATED CARBON FROM APRICOT STONES

A THESIS SUBMITTED TO
THE GRADUATE SCHOOL OF NATURAL AND APPLIED SCIENCES
OF
THE MIDDLE EAST TECHNICAL UNIVERSITY

BY

NEZİH URAL YAĞŞİ

IN PARTIAL FULFILLMENT OF THE REQUIREMENTS FOR THE DEGREE OF
MASTER OF SCIENCE
IN
THE DEPARTMENT OF CHEMICAL ENGINEERING

APRIL 2004

Approval of the Graduate School of Natural and Applied Sciences

Prof. Dr. Canan Özgen
Director

I certify that this thesis satisfies all the requirements as a thesis for the degree of Master of Science.

Prof. Dr. Timur Doğu
Head of Department

This is to certify that we have read this thesis and that in our opinion it is fully adequate, in scope and quality, as a thesis and for the degree of Master of Science.

Prof. Dr. Hayrettin Yücel
Supervisor

Examining Committee Members

Prof. Dr. Suzan Kıncal

Prof. Dr. Zeki Aktaş

Prof. Dr. Güniz Gürüz

Dr. Cevdet Öztin

Prof. Dr. Hayrettin Yücel

ABSTRACT

PRODUCTION AND CHARACTERIZATION OF ACTIVATED CARBON FROM APRICOT STONES

Yağşi, Nezih Ural

M.Sc. Department of Chemical Engineering

Supervisor: Prof. Dr. Hayrettin YÜCEL

April 2004, 114 pages

In this study, characterization of activated carbon produced from apricot stones by chemical activation technique using phosphoric acid (H_3PO_4) as activating agent, at relatively low temperatures (300, 400 and 500°C), was investigated. To produce activated carbon acid impregnated samples were heated; at a heating rate of 20°C/min to the final carbonization temperatures, 300°C, 400°C and 500°C. For each temperature four different carbonization time (90, 120, 180 and 210 min.) were used to produce twelve different activated carbons.

The pore structures of activated carbons were determined as follows: The volume and area of macropores in the pore diameter range of 8180-50 nm were determined by mercury intrusion porosimetry. Mesopore (in the range of 50-2 nm) areas and volumes were determined by N_2 gas adsorption technique at -195.6°C, BET surface areas of the samples were also determined, in the relative pressure range of 0.05 to 0.02, by the same technique. The pore volume and the area of the micropores with diameters less than 2 nm were determined by CO_2 adsorption measurements at 0°C by the application of Dubinin Radushkevich equation.

N_2 (BET) and CO_2 (D-R) surface areas of the samples were in the range of 444-709m^2/g and 433-650m^2/g, respectively. AC4.2 sample (carbonization temperature of 400°C and carbonization time of 120 min.) was found to have the maximum BET and CO_2 area as 709m^2/g and 650m^2/g, respectively.

Surface areas of the samples consisting of around 10% mesopores and over 90% micropores. N_2 adsorption isotherms also confirm that pores are in the micropore range.

Keywords: Activated Carbon, Apricot Stones, Pore Structure, H_3PO_4 Activation

ÖZ

KAYISI ÇEKİRDEĞİNDEN AKTİF KARBON ÜRETİMİ VE KARAKTERİZASYONU

Yağşi, Nezih Ural

Yüksek Lisans, Kimya Mühendisliği Bölümü

Danışman: Prof. Dr. Hayrettin YÜCEL

Nisan 2004, 114 sayfa

Bu çalışmada, kimyasal aktivasyon tekniği ile aktive edici madde olarak fosforik asit (H_3PO_4) kullanılarak oldukça düşük sıcaklıklarda (300, 400 ve 500°C) kayısı çekirdeğinden üretilen aktif karbonun karakterizasyonu incelendi. Aktif karbon üretmek için asit emprenye edilmiş örnekler 20°C/dak. ısıtma hızıyla son karbonizasyon sıcaklığı olan 300°C, 400°C ve 500°C ye ısıtıldı. Her bir sıcaklık için dört farklı karbonizasyon zamanı (90, 120, 180 ve 210 dak.) kullanıldı. Sonuçta, oniki değişik aktif karbon bu yöntemle elde edildi.

Aktif karbonların gözenek yapıları şöyle belirlendi: Gözenek çapları 8180-50 nm arasında olan makrogözeneklerin hacmi ve yüzey alanı civa (intrusion) porozimetresi ile belirlendi. Mezogözenek (50-2nm arasındaki) yüzey alanları ve hacimleri -195.6^{o}C de N_2 gaz adsorbsiyon tekniği kullanılarak belirlendi, BET yüzey alanları da 0.05-0.02 bağıl basınç aralığında aynı teknikle belirlendi. Yarıçapları 2 nm den küçük olan mikrogözeneklerin gözenek hacmi ve yüzey alanı 0°C de CO_2 adsorpsiyon ölçümleriyle Dubinin-Raduskhevic denkleminin kullanılmasıyla elde edildi.

Oniki aktif karbonun yüzey alanları 444-709 m^2/g değerleri aralığında bulunmuştur. Ürünlerin CO_2 (D-R) yüzey alanları 433-650 m^2/g değerleri aralığında çıktığı saptanmıştır. Bu aktif karbonlar içinden maksimum BET ve CO_2 alanı değerleri sırasıyla 709m^2/g ve 650m^2/g olarak AC 4.2 örneğinden (karbonizasyon sıcaklığı 400°C ve karbonizasyon zamanı 120 dak.) bulundu.

Aktif karbonların gözenek yapıları yüzde 10 civarında mezogözenekler ve yüzde 90'ın üzerinde mikrogözeneklerden oluşuyor. N_2 adsorpsiyon izotermleri de gözeneklerin mikrogözenek aralığında olduğunu kanıtlıyor.

Anahtar Kelimeler: Aktif Karbon, Kayısı Çekirdeği, Gözenek Yapısı, H_3PO_4 Aktivasyonu

To My Family,

ACKNOWLEDGEMENTS

It is impossible to acknowledge here individually all the faculty and colleagues and dear friends who contributed in my preparation of this thesis, to whom I extend my thanks and appreciation.

I am very grateful to my thesis supervisor Prof. Dr. Hayrettin Yücel for all his understanding, support and sound advice in all aspects of my research work. I am very much obliged for his objective and tolerant attitude, creating very pleasant working conditions.

I should mention, Alper Uzun, Necati Günaydın, Evren Güner, Berker Fıçıcılar, Onur Diri, Işık Aşar, Umut Barış Ayhan, Murat Üner, Hakan Altındağ, İsmail Doğan, Mustafa Esen Martı, Zeynep Obalı, Kerim Yapıcı, Yalçın Yıldız, Elif Özdemir, my laboratory mate Wisam Abdallah and many others that I could not mention here, who gave me helpful suggestions for the improvement of the document and moral support.

I would like to thank Prof. Dr. Zeki Aktaş (from Ankara University), Ms. Gülten Orakcı, Ms. Mihrican Açıkgöz, Ms. Kerime Güney, Mr. Turgut Aksakal and Mr. Selahattin Uysal for their help in the chemical and physical analysis of the samples.

TABLE OF CONTENTS

ABSTRACT III

ÖZ V

DEDICATION VII

ACKNOWLEDGEMENTS VIII

TABLE OF CONTENTS IX

LIST OF TABLES XIII

LIST OF FIGURES XIV

LIST OF SYMBOLS XVI

CHAPTER

1. INTRODUCTION 1

2. LITERATURE SURVEY 6

2.1. Pyrolysis 6

2.2. Studies on Chemical Activation 8

2.3. Studies on Physical Activation 12

3. ACTIVATED CARBON 16

3.1. Definition and Properties 16

3.2. Principle of Activation Process 18

3.2.1. Raw Materials 18

3.2.2. Production Methods 20
3.2.2.1. Chemical Activation 21
3.2.2.2. Physical Activation 23
3.3. Physical Structure of Activated Carbon 27
3.4. Chemical Properties of Activated Carbon 29
3.4.1. Oxygen Containing Functional Groups 30
3.4.2. Hydrogen Containing Functional Groups 31
3.5. Pore Structure of Activated Carbon 32
4. METHODS USED IN PHYSICAL CHARACTERIZATION OF ACTIVATED CARBON 34
4.1. General 34
4.2. Adsorption Phenomena and Standard Isotherms 36
4.2.1. The Brunauer, Emmett and Teller (BET) Theory 38
4.2.2. Pore Analysis by Adsorption / Desorption 40
4.2.3. Characterization of Microporosity 44
4.3. Mercury Intrusion Porosimetry 47
4.4. Density and Total Pore Volume Determinations 48
5. EXPERIMENTAL WORK 50
5.1. Properties and Preparation of Apricot Stones 50
5.1.1. Properties of Apricot Stones 50
5.1.2. Preparation of Apricot Stones 51
5.2. Carbonization Experiments 52
5.2.1. Experimental Set-Up 52
5.3. Characterization of the Products 54
5.3.1. Nitrogen Gas Adsorption Measurements 56
5.3.2. CO_2 Gas Adsorption Measurements 57
5.3.3. Mercury Porosimetry 59

5.3.4. True Density and Total Pore Volume Determinations 60
6. RESULTS AND DISCUSSION 62
6.1. Chemical Analysis of Products 63
6.1.1. Carbon Content 63
6.1.2. Oxygen and Hydrogen Content 64
6.1.3. Nitrogen Content 66
6.1.4. Ash content 66
6.2. Physical Characterization of the Products 67
6.2.1. Nitrogen Gas Adsorption Measurements 67
6.2.2. Carbon Dioxide Gas Adsorption Measurements 72
6.2.3. Characterization of Activated Carbons by Mercury Intrusion Porosimetry 76
6.3. TGA of Raw and Impregnated Apricot Stones 81
7. CONCLUSIONS 84
8. RECOMMENDATIONS 86
REFERENCES 86
APPEDICES
A. ANALYSIS OF MERCURY POROSIMETRY DATA 91
A.1. Analysis of Macropores 91
A.2. Determination of Apparent Density 93
A.3. Sample Calculation 94
A.3.1. Calculation of Macropore Volume and Area 95
A.3.2. Calculation of Apparent Density 95
B. ANALYSIS OF N_2 SORPTION DATA 96
B.1. Analysis of Mesopores 96
B.2. Determination of BET Surface Area 101
B.3. Sample Calculation 102

B.3.1. Calculation of Mesopore Volume and Area 102

B.3.2. Calculation of BET Surface Area 103

C. ANALYSIS OF CO_2 ADSORPTION DATA 104

C.1. Analysis of Micropores 104

C.2. Sample Calculation 105

D. ANALYSIS OF HELIUM PYCNOMETER DATA 107

D.1 Determination of True Density 107

D.2. Sample Calculation 109

E. TABULATED FORM OF CHEMICAL COMPOSITIONS OF

ACTIVATED CARBONS 110

F. TGA FIGURES OF RAW AND IMPREGNATED APRICOT STONES..... 111

LIST OF TABLES

Table

1.1 Pore Sizes of Activated Carbon 3

3.1 Fixed Carbon Contents of Raw Materials Employed in Activated Carbon Manufacture. 19

5.1 Chemical Composition of Apricot Stones.....51

5.2 Experimental Conditions and Samples Codes. 54

6.1 Mercury Porosimetry Results of Activated Carbons.....77

6.2 Pore Volume Distributions of Activated Carbons 78

6.3 Densities and Total Pore Volumes of Products 80

6.4 Comparison of Total Pore Volumes of the Samples.....81

6.5 Yield Values (%) of Samples for T=300°C.....82

6.6 Yield Values (%) of Samples for T=400°C.....82

6.7 Yield Values (%) of Samples for T=500°C.....82

E.1 Chemical Compositions of Activated Carbons 110

LIST OF FIGURES

Figure

3.1 Pore Structure of Activated Carbon (TEM) 17

3.2 Schematic Representation of (a) Nongraphitizing and (b)Graphitizing Structure of Activated Carbon 27

3.3 Carbon Atom Arrangements in Graphite Crystal 28

4.1 Micropore, Mesopore and Macropore Regions of Activated Carbon 35

4.2 Schematic Representations of Different Types of Adsorption Isotherm 37

4.3 Types of Adsorption-Desorption Hysteresis Loops 43

4.4 Block-Diagram of the Overall Experimental Approach 49

5.1 Experimental Set-Up 53

5.2 Procedure Followed in Experiments 56

5.3 Schematic Representation of Surface Analyzer 58

5.4 Schematic Diagram of Helium Pycnometry 61

6.1 Chemical Compositions of Activated Carbons 65

6.2 BET Surface Areas of the Samples 68

6.3 BJH Meseopore Areas of the Samples 69

6.4 Mesopore Volumes of the Samples 70

6.5 N_2 Adsorption/Desorption Isotherms of AC3 Series 71

6.6 N_2 Adsorption/Desorption Isotherms of AC4 Series 71

6.7 N_2 Adsorption/Desorption Isotherms of AC5 Series 72

6.8 Micropore Area Values From CO_2 Adsorption at 0°C.....73

6.9 Micropore Volume Values From CO_2 Adsorption at 0°C.....74

6.10 Comparison of BET and D-R Results 75

6.11 True Density Values of the Activated Carbons 79

F.1 TGA Result of Acid Impregnated Sample for T=300°C 111

F.2 TGA Result of Acid Impregnated Sample for T=400°C..... 112

F.3 TGA Result of Acid Impregnated Sample for T=500°C 112

F.4 TGA Result of Raw Apricot Stones Sample for T=300°C 113

F.5 TGA Result of Raw Apricot Stones Sample for T=400°C 113

F.6 TGA Result of Raw Apricot Stones Sample for T=500°C 114

LIST OF SYMBOLS

A_m : Cross-sectional area of the adsorbate

C : A constant in equation 4.2

CSA_{N2} : Cross sectional area of nitrogen molecule

D_p : Pore diameter, μm

E_i : Adsorption potential

ΔG : Gibbs free energy change of the reaction

I : Intercept of the BET plot

K : A constant in equation C.1

M : Adsorbate molecular weight, g/mol

n : Amount adsorbed in moles

N_A : Avagadro's constant, $6.023*10^{23}$ molecules/mol

P_i : Partial pressure of the gas, i

P : Pressure, atm, Pa, psia, mmHg

P_0 : Saturation pressure, mmHg

q_1 : Heat of adsorption of the first layer

q_2 : Heat of adsorption of the second and subsequent layers

R : The gas constant, $8.314x10^7$erg/mole-K, $8.314x10^{-3}$ KJ/mole-K

r_p : Actual pore radius, mean radius of the liquid meniscus, nm or μm

r_K : Kelvin radius

r_{KAVE} : Average Kelvin radius

r_{PAVE} : Average pore radius

S : Slope of the BET plot

S_{BET} : BET surface area

S_{cum} : Cumulative pore surface area m^2/g

S_{macro} : Macropore surface area m^2/g

S_{meso} : Mesopore surface area m^2/g

t : Thickness of the adsorbate layer

t_m : Thickness of the monolayer

T : Temperature, °C

T_c : Critical temperature of the adsorption, °C

V : Volume adsorbed, cm^3/g

V_p : Volume of the penetrometer, cm^3

V_s : Volume of the sample, cm^3

V_0 : Micropore Volume, cm^3/g

V_{cum} : Cumulative volume, cm^3/g

V_{Hg} : Volume of the mercury, cm^3

V_m : Monolayer volume, cm^3/g

V_{macro} : Macropore volume, cm^3/g

V_{meso} : Mesopore volume, cm^3/g

V_{mol} : Molar volume of the nitrogen, 34.6×10^{24} A^3/mol at -195.6°C

ΔV_{gas} : Incremental molar adsorbed gas volume, cm^3/g

ΔV_{Liq} : Incremental molar adsorbed liquid volume, cm^3/g

W_0 : Limiting adsorption space volume value

W_a : The quantity of adsorbed at a particular relative pressure

W_{Hg} : Weight of the mercury, g

W_m : The quantity of adsorbed at correspond to BET monolayer

W_p : Weight of the penetrometer, g

W_s : Weight of the sample, g or mg

Greek Letters

μm : Micrometer (10^{-6} meter)

^{o}A : Angstrom (10^{-10} meter)

ρ : Liquid density, g/cm^3

ρ_{He} : Helium (True Density), g/cm^3

ρ_{Hg} : Mercury (Apparent Density), g/cm^3

θ : Contact angle of mercury, 130° and Fraction of surface occupied by adsorbate

σ : Cross sectional area of a CO_2 molecule

γ : Surface tension

CHAPTER I

INTRODUCTION

Activated carbon is a microcrystalline form of carbon with very high porosity and surface area. It may be visualized as foam solid that has a large surface within a rigid granule or particle structure of relatively small volume. Its chemical structure allows it to preferentially adsorb organic materials and other nonpolar compounds from gas or liquid streams (Balcı, 1992; Lumadede, 2002).

Activated carbon has become one of the most technically important and most widely used adsorbents because of its high adsorptive capacity. Present technology demands a very large production of activated carbons with appropriate characteristics for each particular application. In general, an activated carbon which is used in any of the most common applications must have adequate adsorptive capacity, chemical purity, mechanical strength, etc. Furthermore, all these specifications should coexist with a low production cost.

Activated carbon is obtained from a carefully controlled process of dehydration, carbonization and oxidation of organic substances. It can be

prepared for research in the laboratory from a large number of materials. However, the most commonly used ones in commercial practice are peat, coal, lignite, wood and agricultural by-products such as coconut shell, almond shell, rice husks, etc. (Balcı, 1992).

The pyrolysis of starting material with the exclusion of air and without addition of chemical agent usually results in an inactive material with a specific surface area of the order of several m^2/g and low adsorption capacity. One can prepare a carbon with a large adsorption capacity by activating the carbonized products with a reactive gas. The majority of activated carbon used throughout the world is produced by steam activation (physical activation). In this process, the carbonized product is reacted with steam over 900°C.

Another procedure used in the production of activated carbon involves the use of chemical activating agents before the carbonization step. The most commonly used activating agents are phosphoric acid, zinc chloride and salts of sodium and magnesium etc.. Chemical agents act as dehydration agents and they may restrict the formation of tar during carbonization. Chemical activation is usually carried out at lower temperatures than the simple pyrolysis and the activation process with steam or carbon dioxide. The production at lower temperatures promotes the development of a porous structure, because under these conditions elementary crystallites of smaller dimensions are formed. (Smisek and Cerny, 1970)

Most of the available surface area of activated carbon is nonpolar in nature. However, during production the interaction of surface with oxygen produces specific active sites giving the surface of slightly polar nature. As a

result, carbon adsorbents tend to be hydrophobic and organophilic. (Ruthven, 1984)

According to the IUPAC definition, pores can be distinguished in three groups with respect to their dimensions (Reinose, 1985).

Table 1.1 Pore Sizes of Activated Carbon

Macropores	Pores with diameters larger than 50 nm (500 A°)
Mesopores	Pores with diameters between 2 nm and 50 nm (20- 500 A°)
Micropores	Pores with diameters less than 2 nm (2 A°)

Most activated carbons contain pores of different sizes; micropores, transitional mesopores and macropores. Therefore they are considered as adsorbents with wide variety of applications.

Activated carbon adsorbs molecules from both liquid and gaseous phases depending upon the pore size distribution of the adsorbent and also upon the geometry and size of the adsorbate molecule. In adsorption from the gas phase, mainly microporous carbon is used whereas mesoporous carbon is applied in liquid phase processes. Applications of mesoporous activated carbons include; drinking water purification, waste-water treatment, sweetener discolourization, food and chemical processing. On the other hand, microporous carbons are used for solvent recovery, gasoline emission control, cigarette filters and industrial emission gas treatment (Benaddi, 2000).

The usage of carbon adsorbents depend on their surface area, pore size distribution and chemical surface characteristics. The quality (surface area, pore size distribution and hence adsorptive properties) of activated carbons are directly related to the nature of starting material, the type of the production method and the temperature of production.

Activated carbon may not be pure carbon but also contain some impurities depending on the type of starting material. It must be noted that, the adsorption characteristics of activated carbon for certain uses (such as adsorption of electrolytes and non-electrolytes from solutions) are significantly influenced by even small amounts of ash. Moreover, the adsorption of gases is also influenced by the ash content. Therefore, the raw material should contain as small ash as possible. On the other hand, the raw material must have relatively low cost (Balcı, 1992).

Some of the major raw materials used, are agricultural by-products. Although they have very high volatile content and hence give low yields of activated carbon, they are relatively inexpensive and economical starting materials. In Turkey, abundant amounts of agricultural by products including apricot stones are available.

According to 1998 data of FAO, Turkey is the biggest apricot producer in the world with a 20.15% share with its 538.000 tones production. From this production about 35.000 tones apricot pit and 7.000 tones kernel are obtained annually. (The pit consists of kernel and its encasing shell; however, kernel is just edible part of pit). Approximately 50% of this production comes from the Malatya region (Asma, 2000). On the other hand, in the selection of raw

material, alternative uses of it must be considered together with the economics of the production.

Most of the studies have shown that, activated carbons obtained from agricultural by-products can be favorably compared with other activated carbons used in industry with respect to their adsorptive properties (Balcı, 1992).

The objective of this study is to produce activated carbon from an agricultural waste; apricot stones by chemical activation using phosphoric acid and characterize this product in terms of pore size distribution, pore volume and surface area by BET (Braunauer, Emmet, Teller) method, BJH (Barrett, Joyner, Hallenda) Method, DR (Dubinin, Radushkevich) Method, Helium Pycnometer and Mercury Intrusion Porosimeter.

The major novelty of this work is the production of activated carbons from phosphoric acid impregnated apricot stones samples by chemical activation technique in a temperature range of 300°C to 500°C.

CHAPTER II

LITERATURE SURVEY

Activated carbon is one of the most commonly used adsorbents in many industrial applications for its adsorptive capacity. In this study, production of activated carbon from apricot stones and the quality of the products have been investigated.

2.1. Pyrolysis

As lignocellulosic materials are heated in an inert atmosphere, they decompose to various pyrolysis products. Depending on their volatility, these products can be grouped into three classes; chars, gases and tars. Char is a carbon-rich nonvolatile solid residue, usually constituting approximately 15-20 percent yield. Gas phase products include all lower molecular weight products (CO, CO_2, CH_4, H_2, etc.) including water. Usually gas phase products constitute 20-25 percent of the total products of pyrolysis. Tars are any of several high molecular weight products that are volatile at carbonization temperatures but condense onto any surface near room temperature. Tar comprises

approximately 60-65 percent of the products (Schwenker and Pascu, 1957; Roberts, 1970; Agrawal and Mc Cluskey 1983). Any one of the pyrolysis products could be the most desirable product. Most commercial scale pyrolysis plants are designed to have only one class as the principal product with at least one of the other classes serving as a fuel source. For manufacture of activated carbon, the char is the desirable product.

Pyrolysis of lignocellulosic materials such as shells or stones of fruits etc. is extremely complex. The major components, lignin, cellulose and hemicellulose mainly react independently and the pyrolysis of the lignocellulosic materials is the result of hundreds of cocurrent and consecutive reaction. In order to investigate mechanism of pyrolysis, it is better to study pyrolysis of each component separately. Cellulose is the major components of plants cell and hemicelluloses have approximately the similar molecular structure with cellulose. So investigation of cellulose pyrolysis mechanism gives an idea about the pyrolysis of lignocellulosic materials. Pyrolysis of pure cellulose has been widely studied. During heating in an inert atmosphere, molecular bonds will be broken. Since C-O bonds are weaker than the C-C bonds the principal candidates for scission are the 1,4 C-O-C glucosidic and the 1,5 C-O-C acetal linkages in the cellulose macromolecule. The breakage of 1,4 glucosidic bonds results in depolymerization of cellulose and is responsible for the formation of tars. As discussed by Agrawal (1988 a,b) the breakage of 1,5 acetal bonds leads to ring opening and results in formation of gases and chars.

The influence of the experimental conditions such as temperature, heating rate, residence time at high temperature can be interpreted in terms of competition between these two types of cellulose degradation. At temperatures

below about 300°C, the ring opening reaction is favored over depolymerization. Higher heating rates cause temperatures favorable to depolymerization to be reached more quickly, and hence give higher tar yield. Trace amount of impurities are thought to catalyze the ring opening reactions. (Agrawal and Mc Cluskey, 1983)

The production of activated carbon is a typical gas-solid reaction. The adsorptive capacities of activated carbon are mainly associated with its internal pore properties such as pore surface area, pore volume and pore size distribution, which develop during the activation of chars.

2.2. Studies on Chemical Activation

Bevla et al. (1984 a,b) produced activated carbon from almond shells through chemical activation. From several activating agents (H_3PO_4, $ZnCl_2$, K_2CO_3 and Na_2CO_3), $ZnCl_2$ activation gave the best products with high adsorption capacities. On the other hand, they observed that, adsorption capacities, N_2- BET surface area values and iodine numbers decreased with the decrease of particle size.

Laine et al. (1989) prepared activated carbons from untreated and phosphoric acid treated coconut shells. Carbonization of the shells, activation in N_2-forced and O_2-forced flow production methods were carried out in the muffle furnace. The optimum production temperature for a higher surface area was observed as 450°C. The products obtained under the forced flow showed a decrease in surface area and yield.

Blasco et al. (1990) studied the kinetics of thermal decomposition of untreated and chemically treated holm oak wood using thermogravimetry technique. They used sulphuric acid, phosphoric acid and zinc chloride as the chemical agents. The weight changes with temperature were measured to obtain activation energy distribution. They found that the activation energy distribution of pyrolysis of untreated and H_2SO_4 treated wood samples were quite similar. In the case of $ZnCI_2$ treated wood, due to the early dehydration reactions, significant weight loss at relatively low temperatures was observed.

Balcı et al. (1994) prepared activated carbon from ammonium chloride-impregnated and untreated almond shell and hazelnut shell samples. They carbonized samples in a flow of nitrogen at relatively low temperatures. It was observed that, chemical activation carried out at 350°C gave products with surface area values above 500 m^2/g. However, the surface area values observed for the products obtained from untreated raw materials were about half of this value. It was also observed that, the surface area of products obtained from NH_4Cl-impregnated samples reached values of over 700m^2/g when the carbonization temperature was increased 700°C.

Toles et al. (1997) prepared activated carbon from almond and pecan shells, which were hard, lignocellulosic precursors for the production of granular activated carbon (GACs) in order to create carbons for the adsorption of both organic compounds and metals. They activated samples either chemically, with H_3PO_4, or physically, with CO_2, under a variety of conditions. The product obtained by chemical activation had higher BET surface areas and greater product yields than the CO_2-activated carbons. They also compared the products with the commercial activated carbon with respect to adsorption ability.

Girgis et al. (1998) carbonized phosphoric acid impregnated apricot stones at 300 400 and 500°C respectively. For impregnation, a ratio of acid volume: weight of raw precursor of 1.5/1 was employed and it was observed that, as the temperature increased the BET surface area increased from 700 m^2/g up to 1400 m^2/g. In this study, they used 20%, 30%, 40% and 50% (vol) phosphoric acid. The highest BET surface area was obtained from the sample which was impregnated with 30% (vol) phosphoric acid and carbonized at 500°C.

Toles et al. (2000) prepared a series of phosphoric-acid activated carbons made from almond shells using six different activation or activation/oxidation methods. They compared the carbons to each other and to two commercial carbons in an effort to ascertain the relative value of the carbons in terms of yield, surface area, attrition, surface functional groups, organic uptake, metal uptake, as well as estimated cost of production. Of the six methods investigated, the method that produced the best overall performing almond shell carbon and least expensive carbon in terms of production cost was the "Air-Activation" method. This method involved the simultaneous activation and oxidation of almond shells under an air atmosphere.

Hu et al. (2001) used coconut shells and palm seeds as raw materials to obtain activated carbons with high surface area by simultaneous treatment with zinc chloride and carbon dioxide as the chemical and physical agents, respectively. They observed that, both the surface area and the mesopore content could be tuned by controlling the experimental parameters, i.e., $ZnCl_2$-to-raw material ratio, duration of exposure to the carbondioxide atmosphere and temperature of activation. They found $ZnCl_2$-to-shell ratios above 1 yielded high

surface areas, and ratios above 2 resulted in high mesopores content. They investigated the adsorption capacity and nature of the porosity by adsorption experiments using adsorbates with different molecular sizes. They noticed that, the capacities of the mesoporous activated carbon were much higher than those of microporous carbon for larger adsorbates, confirming the presence of large amounts of mesopores in the former.

Iniesta et al. (2001) pre-treated almond shell samples with both basic and acidic treatments for varying lenghts of time (10% of sulphuric acid and 2% of sodium hydroxide at 30 min., 1, 3 and 24 h). They analysed combined acidic-basic as well as basic-acidic treatments, and amount of ashes of each sample. They carbonised different samples in a reactor to study the effect of the acidic pre-treatments on the char yields. They studied on the reactivity of the samples by thermogravimety under CO_2 atmosphere. They found that, the samples pre-treated with acid showed a lower reactivity than the untreated and basic-treated samples, as a consequence of the lower amount of ashes, thus reducing their catalytic effect. Additionally, they observed that, at low temperature of carbonisation such samples resulted in higher yields as a consequence of the relatively higher lignin fraction remaining in those samples (acidic treatment partly removes the hemicellulose and cellulose fractions).

Özer et al. (2002) produced activated carbon from sugar beet pulp treated with phosphoric acid (30%) and carbonized at different temperatures (300-500°C) and time (90, 120, 180, 300 min). It was obtained that, the BET surface area value of activated carbon increases with an increase in temperature and time of carbonization. The highest BET value, (104.6m^2/g) was obtained

when carbonization temperature was 500°C and carbonization time was 300 min.

Basso et al. (2002) produced activated carbons from canes from Arundo donax, a rapid-growing plant, by phosphoric acid activation under four different activation atmosphere, to develop carbons with substantial capability to adsorb Cd(II) and Ni(II) ions from dilute aqueous solutions. Surface areas and total pore volumes of the activated carbons they used were of around 1100 m^2/g and 1 cm^3/g, respectively. They observed that, the content of carbons' polar or acidic surface oxygen functional groups, with their development depending on the atmosphere used, influenced predominantly metal adsorption. They also found that, carbons derived under flowing air, possesing the largest total content of these groups, showed the best adsorption effectiveness (>90%) for both ions, even superior to that determined for a commercial sample used as a reference.

2.3. Studies on Physical Activation

Solano et al. (1980) produced activated carbon from direct activation of almond shells with CO_2 or air, or by activation after carbonization under nitrogen atmosphere. It was observed that, direct activation with carbon dioxide in the temperature range of 750°C and 900°C gave activated carbons with similar or larger surface area and micropore volumes than those obtained by carbonization followed by activation. The products obtained by the activation of air in the temperature range from 300 to 400°C, did not show large surface areas. It was also observed that, at low temperatures direct activation with air developed meso and macroporosity to a larger extent than the activation which

was preceded by carbonization. However, the reverse case was observed for the high temperature products. The products had surface areas ranging from 150 m^2/g to about 2000 m^2/g for different degree of burn off and types of production.

Reinoso et al. (1985) prepared activated carbons from plum and peach stones by carbonization followed by carbon dioxide activation with activation time ranging from 8 hours to 16 hours. The adsorption of N_2, CO_2, i-butane, paranitrophenol and methylene blue had been studied to investigate the microporosity. N_2 adsorption studies gave the micropore volumes ranging from 0.27 cm^3/g to 0.77 cm^3/g for products from plum stones and 0.23 cm^3/g to 0.38 cm^3/g for those obtained from peach stones for various production methods and conditions. Porosimeter results showed that, macro and meso porosities were more developed in carbons prepared from plum stones. Direct activation led development of these two ranges of porosity, especially macro porosity to larger extents.

Perez et al. (1991) studied characterization of the products obtained from CO_2-activation of almond shells with different burn off ranging from 29 percent to 82 percent. First almond shells were carbonized in argon atmosphere then activated. N_2, CO_2 and n-butane adsorption and n-nonane preadsorption characterization techniques showed that, the increase in percent burn off caused an increase in the amount adsorbed and widening of micropore size distribution.

Sanchez et al. (2001) prepared three series of activated carbons from *Quercus agrifolia* wood using a two-step process, carbonization followed by physical activation with CO_2. They characterized samples by N_2 and CO_2

adsorption. They used three activation temperatures, 800, 840 and 880°C, covering the 18–85 wt % yield range by variation of residence time. They obtained activated carbons with a well-developed porous structure, predominantly microporous with high BET surface areas. They found no direct relationship between exposed BET surface areas (the surface where activation reaction takes place), evolution and gasification rate variation. They noticed that, porosity development appeared to be strongly influenced by the kinetic reaction stage and the reactant gas concentration gradient had being an ultimate factor that induced porosity evolution. They produced activated carbons which BET surface areas were in the range of 400-1200 m^2/g.

Baçaoui et al. (2001) prepared a series of activated carbons from olive-waste cakes by physical activation with steam. They carried out adsorption of N_2 (-195.6°C), CO_2 (0°C) and mercury porosimetry experiments to determine the characteristics of all carbons prepared. They found experimental response varied between: 13–27% for the total yield, 115–490 mg/g for the adsorption of methylene blue, 741–1495 mg/g for the adsorption of iodine, 514–1271 m^2/g for the BET surface area, 0.225–0.377 cm^3/g for the micropore volume, 0.217–0.557 cm^3/g for the volume of pores with a diameter greater than 3.7 nm and 31.3–132 m^2/g for the external surface area. They exploited the results obtained using response surface methodology. They represented these responses and studied in all experimental regions of activation time and activation temperature, the most influential factors in activated carbon preparation. They obtained the optimal activated carbon when using 68 min as activation time and 822°C as activation temperature.

Yang et al. (2003) produced activated carbons from pistachio-nut shells, which are one type of lignocellulosic material, by a two-step physical method. They studied on the effects of the preparation variables on the activated carbon pore structure, followed by the optimization of these operating parameters. They found that the activation temperature and dwell time are the important parameters that affect the characteristics of the activated carbons obtained. They were studied the effects of CO_2 flow rate and heating rate during activation. Under the experimental conditions used, the optimum conditions to prepare activated carbons with high surface area and pore volume were identified. They examined the microstructure of the activated carbons by scanning electron microscopy while the Fourier transform infrared spectra showed the changes in the surface functional groups produced during the different preparation stages.

CHAPTER III

ACTIVATED CARBON

3.1. Definition and Properties

Activated carbon is a microcrystalline, nongraphitic form of carbon. X-ray analysis of activated carbons shows a structure which is much more disordered than that of graphite, having crystallites only a few layers in thickness and less than 10 nm in width (Smisek and Cerny, 1970). The spaces between the crystallites of activated carbon constitute the microporous structure with a large internal surface area of 250 m^2/g-2500m^2/g. Because of the chemical structure of activated carbon it can preferentially adsorb organic materials and other nonpolar compounds from the gas or liquid streams. Due to these properties, they have been used for the purification of gases, the separation of gas mixtures, the purification of exhausted air, especially the recovery of solvents, the removal of heavy metals, and the decoulorization of solutions and the purification of water for many decades. Carbonaceous adsorbents found greater use in the solution of environmental problems related to water purification and removal of air pollutants. (Smisek and Cerny, 1970; Hassler, 1974)

The removal of impurities from gases and liquids by activated carbon takes place by adsorption. Adsorption is a term which describes the existence of a higher concentration of a substance at the interface between a fluid and a solid than is present in the fluid. Pore structure of activated carbon (from TEM) is shown in Figure 3.1.

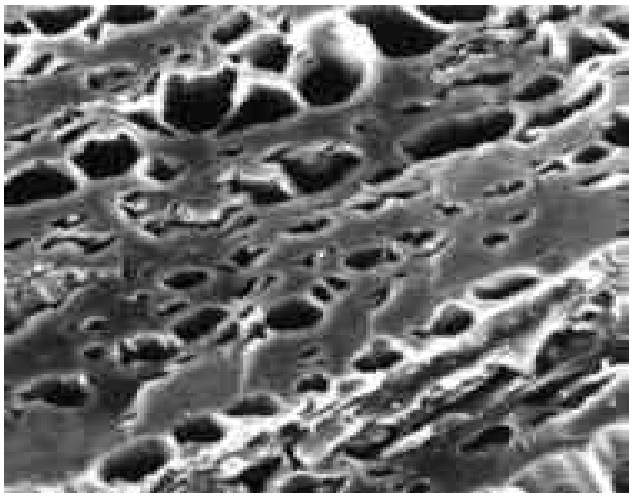

Figure 3.1 Pore Structure of Activated Carbon (TEM)

Adsorption process can be considered as either chemisorption or physical adsorption. In physical adsorption the impurities are held on the surface of the carbon by weak van der Waals forces while in chemisorption, the forces are relatively strong and adsorption occurs at active sites on the surface. Therefore, in chemisorption the efficiency of carbon will depend upon its accessible surface area and also upon the presence of active sites on the surface where chemisorption may occur. (In physical adsorption accessible surface area and the presence of active sites on the surface are not important.)

The porous structure and chemical nature of an activated carbon is a function of the raw materials used in its preparation and the activation method

used. This is the reason why surface area or pore volume of activated carbons can vary widely from one kind to another.

3.2. Principle of Activation Process

The principle of manufacturing carbonaceous adsorbents is the selective removal of some groups of compounds from a suitable carbon containing material and generation of a highly porous solid matrix containing micropores. Removal of such compounds can be achieved by the carbonization and activation of the raw materials. But in chemical activation method there is no activation step.

3.2.1. Raw Materials

The quality of the resulting activated carbon is considerably influenced by the raw material. Although the activation procedure employed mainly determines the chemical nature of the surface oxides and the surface area of the resultant product, the structure of the pores and the pore size distributions are largely predetermined by the nature of the starting material. Any cheap substance with a high carbon and low ash content can be used as a raw material. Raw materials for the production of activated carbon include number of carbonaceous materials, apricot stones, wood, peat, brown coal, bituminous coal, lignite, coconut shells, almond shells, pits from peaches and other fruit, petroleum-based residues and pulp mill residues (Balcı, 1992).

Since the manufacturing process involves the removal of volatile matter, the economic relationship between price, availability and quality of raw

materials on one side and volatile content on the other side, is an important one. The most important advantages of using bituminous coal and anthracite are their relatively low volatile content and hence high yield of product.

Fixed carbon contents of some raw materials are given in Table 3.1. On the other hand, the younger fossil materials-wood, (mainly birch wood and beech wood) peat and wastes of vegetable origin (such as apricot stones, almond shell, coconut shell, saw dust) can be activated easily and give high quality products. (Smisek and Cerny, 1970; Martin, 1981; Holden, 1982)

Table 3.1 Fixed Carbon Contents of Raw Materials Employed in Activated Carbon Manufacture (Holden, 1982).

Material	Percent Carbon Content
Soft Wood	40
Hard Wood	40
Coconut Shell	40
Lignite	60
Bituminous Coal	75
Anthracite	90

3.2.2. Production Methods

Activated carbon can be prepared by one of the following two methods:

1. By carbonizing material of vegetable origin with the addition of activating agents which influence the course of carbonization. The method is generally known as "chemical activation".

2. By allowing the inactive carbonized product prepared by the usual methods of carbonization to react with suitable, usually gaseous (generally steam or carbon dioxide) substance. This procedure is known as "physical activation" or "gas activation".

Chemical activation is used generally when raw materials with a recent origin (currently grown) are dealt with (Balcı, 1992).

The basic production processes can be combined in different ways. Sometimes the chemically activated carbon is subjected to additional activation with gaseous environment in order to change the pore structure of the final product.

In contemporary technologies both types of activation, chemical and physical are widely used. Although high quality products can be obtained by both procedures, sometimes, they are not equally good for all purposes. For example, for the recovery of solvent, chemically activated carbons are preferred, whereas for water treatment, carbon activated with steam appears to be preferable. (Smisek and Cerny, 1970)

3.2.2.1. Chemical Activation

Activated carbon can be prepared by chemical activation. In this method, the carbonaceous material is carbonized after the addition of substances which restrict the formation of tar. Used chemical is recovered for reuse and to free the pores after carbonization. Through chemical activation, a carbonized product with very good sorption properties can be obtained in a single operation.

Chemical activation is used almost exclusively for carbons produced from materials of recent origin, namely lignocellulosic materials. The activation agent influences the pyrolytic process. By this technique the formation of tar is restricted to a minimum. The yield of carbon in the carbonized product is increased accordingly. Furthermore, temperature needed for pyrolysis is also lower than that needed for activation with gaseous agents in physical activation, and this promotes the development of a porous structure. Under these conditions elementary crystallites of smaller dimensions, (micropores) are formed (Balcı, 1992).

The most widely used activation agents are phosphoric acid, zinc chloride and potassium sulphide. In some studies hydroxides of an alkali metal, magnesium and calcium chloride and other substances are also used. All these chemicals are strong dehydrating agents. On calcination, the impregnated chemicals dehydrate the raw materials, which results in changing and aromatization of the carbon skeleton by the creation of a porous structure and surface area.

The material mainly used in the production of activated carbon consists predominantly of cellulose, and therefore in a discussion of the mechanism of chemical activation, the action of the chemical agent on cellulose must first be considered. Cellulose is composed of elongated macromolecules, up to 1800 nm -2000 nm long, orientated in the direction of their longitudinal axes, which form agglomerates known as micelles. The orientated chains of molecules are laterally bounded by bonds of different types of strength. The electrolytic action of the activation agent causes the cellulose to undergo a change known as swelling, during which the arrangement of the molecules in the direction of the longitudinal axis remain unchanged, but the lateral bonds are broken down with the result that the inter-and-intra micelle voids increase until finally the cellulose is dispersed. Simultaneously other reactions, hydrolytic or oxidative, take place, by which the macromolecules are gradually depolymerized. The processes lead to the formation of a homogeneous plastic mass consisting of the partially depolymerized substance uniformly saturated with the activation agent (Browning, 1963, Smisek and Cerny, 1970).

A further aspect of the action of the activation agent is reactions which change the chemical nature of the cellulose substance. The most important of these reactions is dehydration which assists in the decomposition of organic substances by the action of heat and prevents the formation of non-carbonized degradation products (tar).

An important factor in chemical activation is the degree (coefficient) of impregnation. This coefficient is the weight ratio of the anhydrous activation agent to the dry materials. The effect of the degree of impregnation on the porosity of the resulting product is apparent from the fact that the volume of

salt in the carbonized material is equal to the volume of pores which are freed by its extraction. For small degrees of impregnation, the small increase in impregnation amount, causes an increase in the total pore volume of the product showing an increase in the volume of smaller pores. When the degree of impregnation is further raised, the number of larger diameter pores increases and the volume of the smallest pores decreases (Balcı, 1992).

The activated carbons produced through chemical activation, especially when $ZnCl_2$ is used, must be cleaned from the chemical agent before their commercial use. One advantage of using phosphoric acid in chemical activation is that, it can be cleaned from the activated carbon by rinsing with boiling pure water.

3.2.2.2. Physical Activation

a. Carbonization

The method of production of the carbonized intermediate product has a marked effect on the quality of the final activated carbon product. The main aim of carbonization is to reduce the volatile content of the source material in order to convert it to a suitable form for activation. During the phase of the carbonization, carbon content of the product attains a value of about 80 percent.

By carbonization most of the non-carbon elements, hydrogen and oxygen are first removed in gaseous form by pyrolytic decomposition of the starting

material and the freed atoms of elementary carbon are grouped into organized crystallographic formation known as elementary graphitic crystallites.

Carbonization of lignocellulosic material starts above 170°C and it is nearly completed around 500°C- 600°C. In the production of charcoal, it is desirable to carry out its pyrolysis sufficiently quickly, in order to reduce the time of contact of the carbon formed with the decomposition products. The rate of pyrolysis is significantly influenced by the moisture content of the starting material. Further important factors are uniform heating of the retort and the temperature of carbonization which must not be very high.

In the simple carbonization product, the mutual arrangement of the crystallites is irregular, so that free interstices remain between them. However, as a result of deposition and decomposition of tarry substances, these become filled or at least blocked by disorganized (amorphous) carbon. The resulting carbonized product has small adsorption capacity. Presumably, at least for carbonization at lower temperatures, part of the formed tar remains in the pores between the crystallites and on their surface. Such carbonized materials can then be partially activated by removing the tarry products by heating them in a stream of an inert gas, or by extracting them with a suitable solvent, or by a chemical reaction (for example, heating in an atmosphere of sulphur vapor at temperatures lower than those at which reactions with carbon take place). (Smisek and Cerny, 1970; Wigmans, 1985)

b. Activation of Carbonized Intermediate Product with Gaseous Agents

A carbon with a large adsorption capacity can also be produced by activating the carbonized material under such conditions that the activating agent reacts with the carbon. The most common activation agents are steam, carbon dioxide and oxygen (air). Activation step is generally conducted at temperatures between 800°C and 1100°C. The active oxygen in the activating agent basically burns away the more reactive portion of the carbon skeleton as carbon monoxide and carbon dioxide, depending on the gaseous agent employed.

Activation takes place in two stages. In the initial stage, when the burn off is not higher than 10 percent, disorganized carbon is burnt out preferential and the closed and clogged pores between the crystallites are freed. By the removal of disorganized carbon, the surface of the elementary crystallites became exposed to the action of the activation agent. The burning out of the crystallites must proceed at different rates on different parts of the surface exposed to reaction; otherwise new pores could not be formed.

The removal of nonorganized carbon and the non-uniform burn out of elementary crystallites leads to the formation of new pores, and to the development of the macroporous structures. The effect which becomes increasingly significant is the widening of existing pores, or the formation of larger size pores by the complete burn out of walls between adjacent micropores. (Physical structure of activated carbon is discussed in Section 3.3.)

According to the type of the gaseous activation agent, some difficulties may arise. Activation with steam and carbon dioxide are carried out at temperatures between 800°C and 1100°C.

At lower temperatures, reactions are too slow. However, the temperature must be carefully chosen to make the rate determining factor as the chemical reaction between carbon and gaseous agent. In kinetics control region, reactions take place at the interior surface of the carbon. Hence the removing of carbon from the pore walls causes the enlargement of the pores. However at much higher temperatures reactions become diffusion controlled and occurs on the outside of the carbon particle.

The reaction of oxygen with carbon is exothermic. Therefore, for the activation of the carbonized product with oxygen it may be difficult to maintain the correct temperature in the oven. Possible local overheating prevents the uniform activation. Furthermore, due to the very aggressive action of oxygen, burn out is not limited to pores but also occur on the external surface of the grain by causing great loss. It must be noted that, carbon activated with oxygen have a large amount of surface oxides. Due to the difficulties and disadvantages explained, oxygen (air) activation is rarely used.

Generally, carbonization and activation steps are carried out separately, but recently there is an increasing tendency to conduct the two processes together. (Smisek and Cerny, 1970; Hassler, 1974; Wigmans, 1985; Balcı, 1992)

3.3. Physical Structure of Activated Carbon

The structure studies of Franklin (1951) on carbonized materials showed two distinct well defined classes; nongraphitizing carbons and graphitizing carbon (Figure 3.2).

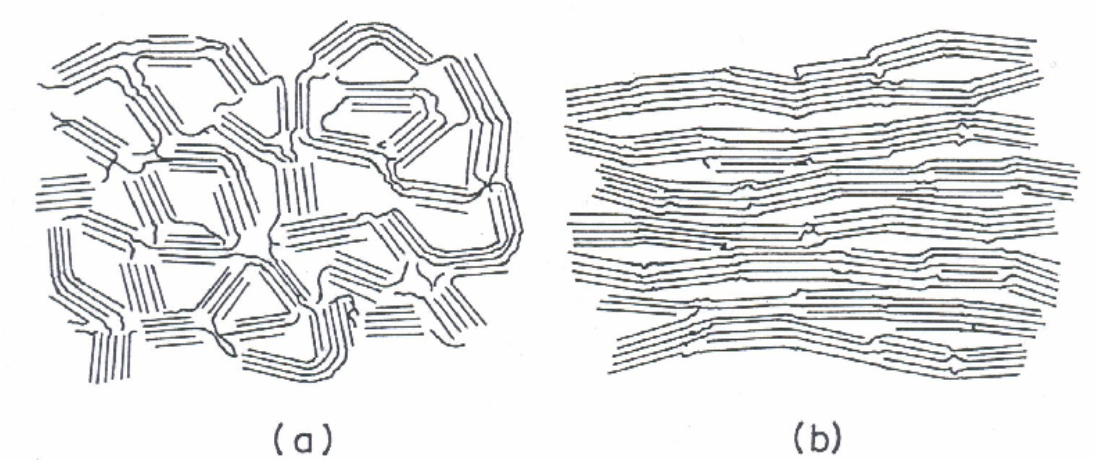

Figure 3.2 Schematic Representation of (a) Nongraphitizing and (b) Graphitizing Structure of Activated Carbon (Smisek and Cerny, 1970)

In general, the nongraphitizing carbons are formed from substances containing little hydrogen or more oxygen. On heating such substances, at low temperature develops a strong system of cross linking of crystallites forming porous mass. The graphitizing carbons are prepared from substances containing more hydrogen. The crystallites remain relatively mobile during the early stages of carbonization and cross linking is much weaker. As a result, softer and less porous carbon is obtained.

The basic structural character of activated carbon is closely approximated by the structure of pure graphite. The graphite crystal is composed of layers of

fused hexagons held approximately 0.335 nm apart by van der Waals forces (Smisek and Cerny, 1970).

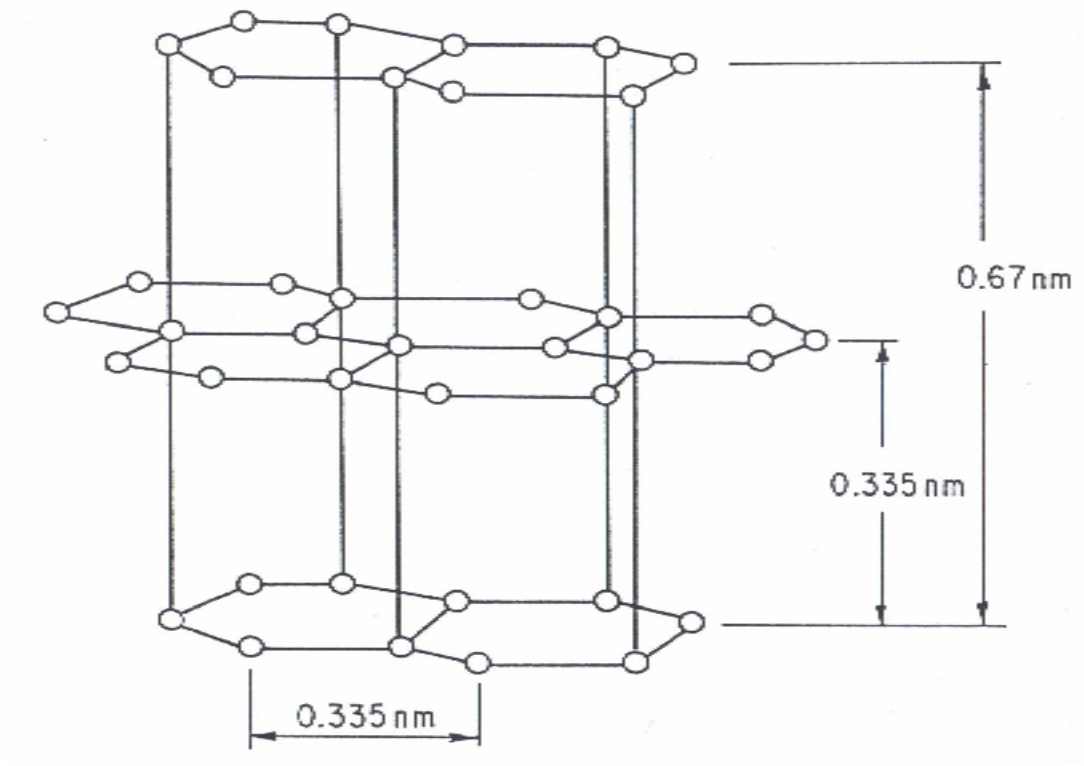

Figure 3.3 Carbon Atom Arrangements in Graphite Crystal

However, the structure of activated carbon differs somewhat from that of graphite. During carbonization process, several aromatic nuclei, having a structure similar to that of graphite are formed. Planar separation distance in carbon is approximately 0.36 nm. From X-ray spectrograph, these structures have been interpreted as microcrystallite consisting of fused hexagonal rings of carbon atoms structurally, carbon can therefore be considered to consist of rigid interlinked cluster of microcrytallites. Each microcrystallite comprises a stack of graphite planes.

Microcrystallites are interconnected by interaction of functional groups terminating the graphitic planes. The diameter of the planes forming the microcrystallites, as well as the stacking height, has been estimated at 2 nm -5 nm indicating that each microcrystallite consists of about 5-15 layers of graphite planes (Wolff,1959).

3.4. Chemical Properties of Activated Carbon

The adsorptive properties of activated carbon are determined not only by its pore structure but also by its chemical composition. Activated carbon contains two types of admixtures. One of them is represented by chemically bonded elements, in the first place oxygen and hydrogen. These are derived from the starting material and remain in the structure of activated carbon as a result of imperfect carbonization or become chemically bonded to the surface during activation.

The other type of admixture consists of ash which is not an organic part of the product. The elemental composition of activated carbon typically comprises 85-90 % C, 0.5 % H, 0.5 % N, 5 % O, and 1 % S, the balance of 5-6 % representing inorganic (ash) constituents. However, these values can not serve as specification for activated carbon's quality or properties (Faust and Aly, 1983).

Surface area generated by the more reactive edges of the microcrystallite will contain a wide variety of functional groups and will accordingly quite heterogeneous in nature. The nature of the relevant functional groups is determined to a large extent by the method of activation as well as by

the type of raw material from which the activated carbon is produced (Cookson, 1980; Wigman, 1985).

3.4.1. Oxygen Containing Functional Groups

The oxygen of starting material has a considerable influence on the arrangement and size of the elementary crystallites formed in carbonaceous adsorbents. In adsorbents prepared from materials of high oxygen content, the distance between the parallel graphitic layers is appreciably smaller. Moreover the course of carbonization and the required carbonization temperature depend very much on the oxygen content of raw material.

On the other hand, if oxidizing gases possess the oxygen, this oxygen also be chemisorbed and bound as surface oxides on the edge of the layer planes. The presence of chemisorbed oxygen on the surface of activated carbon has important effects on its capacity to adsorb water vapor and vapor of other polar adsorbates (Balcı, 1992).

The oxygen content of activated carbon ranges between 1 % and 25 % and has been shown to vary considerably with the activation temperatures. The amount of oxygen decreases with an increase in the activation temperature.

Carbon activated at low temperatures 200°C-500°C, termed as L-carbons, generally will develop acidic surface oxides. The acidic surface oxides could mainly include phenolic hydroxyl groups. The carbons activated by chemical treatment in aqueous solutions with such oxidizing agents as chloride,

permanganate, persulfate, hydrogen peroxide and nitric acid, develop the same characteristics as L-carbon.

The carbons activated at higher temperatures 800°C–1000°C, termed as H-carbons, will develop basic surface oxides. Adsorption of electrolytes is affected by the presence of basic or acidic surface oxides. The presence of surface oxygen complexes will also impart a polar character to the activated carbon surface, which should affect preferential adsorption of comparatively polar organic compounds (Balcı, 1992).

3.4.2. Hydrogen Containing Functional Groups

Materials prior to activation contain hydrogen in the form of hydrocarbon chains and rings attached to border atoms of the hexagon planes. Most of this hydrogen is removed during activation at temperatures below 950°C, but some hydrogen is still held after activation and is not released unless much higher temperatures are reached. It is to be noted that, the evolution of this latter portion of hydrogen at very high temperatures is paralled by a simultaneous decrease in adsorptive power.

Hydrogen is more strongly chemisorbed than oxygen. Infrared studies showed that hydrogen was present in aromatic and aliphatic form. The aromatic hydrogen was suggested to be bonded covalently to the carbon atoms at the periphery of the aromatic basal planes. The aliphatic hydrogen was suggested to be present in the form of aliphatic chains and alicyclic rings attached to the peripheral aromatic rings. In addition to hydrogen and oxygen, calcined sulphur,

nitrogen, chlorine and other elements can also be present in active carbon (Balcı, 1992).

3.5. Pore Structure of Activated Carbon

During the process of activation, the spaces between the elementary crystallites become cleared of various carbonaceous compounds and nonorganized carbon. Carbon is also removed partially from the graphitic layers of the elementary crystallites. The resulting voids are termed as pores. Results seem to indicate that, there are pores with a contracted entrance (ink-bottle shaped) pores in the shape of capillaries open at both ends or with one end closed, pores in the shape of more or less regular slits between two planes, v-shaped, tapered pores, and other forms.

In most cases, however it is difficult to determine the pore shapes reliably. However, the calculation of diameters of pores assuming cylindrical capillary shapes yields values which approach more nearly the actual dimensions of the pores. Activated carbon usually has pores belonging to several groups, each group having a certain range of values for the effective dimensions.

Pores of an effective diameter larger than about 50 nm, are classified as macropores. Their volume in the activated carbon is generally between 0.2 cm^3/g and 0.5 cm^3/g and their surface area is 0.5 m^2/g to 2 m^2/g.

Transitional pores are those in which capillary condensation with the formation of a meniscus of the liquefied adsorbate can take place. This

phenomenon usually produces the hysteresis loop on the adsorption isotherm. The effective diameters of transitional pores are in the range of 2 nm to 50 nm. Their specific surface area is generally around 5 % of the total surface area of the activated carbon.

Pores with an effective diameter of less than about 2 nm are called micropores. The micropore volume is generally around 0.15 cm^3/g to 0.50 cm^3/g. Usually the specific surface area of micropores amounts to over 90 % of the total specific surface area (Gregg and Sing 1967;. Smisek and Cerny, 1970; Rodriguez Reinoso, 1989).

Each of these three groups of pores has its specific function in the process of adsorption on activated carbon. According to the type of application, the percentages of the transitional pores and the micropores could be adjusted employing special production procedures.

CHAPTER IV

METHODS USED IN PHYSICAL CHARACTERIZATION OF ACTIVATED CARBON

4.1. General

Conventional classification of pores according to their diameters, originally proposed by Dubinin (1947) and now officially adopted by the International Union of Pure and Applied Chemistry, (IUPAC) is mostly used. (This classification is given in Chapter I.) There are tree commercial types of activated carbon with respect to product dimension; (i) Pellet Activated Carbon which particle sizes are in the range of 0.8-5mm. (ii) Granular Activated Carbon (GAC) which particle sizes are in the range of 0.2-5mm. (iii) Powdered Activated Carbon (PAC) which particle sizes smaller than 0.18mm (or higher than 80 mesh).

There are numerous techniques and methods for the characterization of pore structure of activated carbon. Since by nature the size of the pores vary in a wide range, (e.g. macro, meso, micro) there is not a single technique to provide information in all ranges of pores. Therefore, in most cases a

combination of different methods are used. For the quantitative characterization of the pore structures; estimation of pore surface area, pore volume, and pore size distribution together with the true and apparent density determinations are needed. For this purpose; the adsorption of gases and vapors by standard gravimetric or volumetric techniques and mercury porosimetry are still classical and convenient approaches to the general characterization of porosity in activated carbon. Other, complementary techniques such as, small angle scattering (X-rays or Neutrons), transmission electron microscopy, etc. are also used or the characterization of pores. (Şenel, 1994)

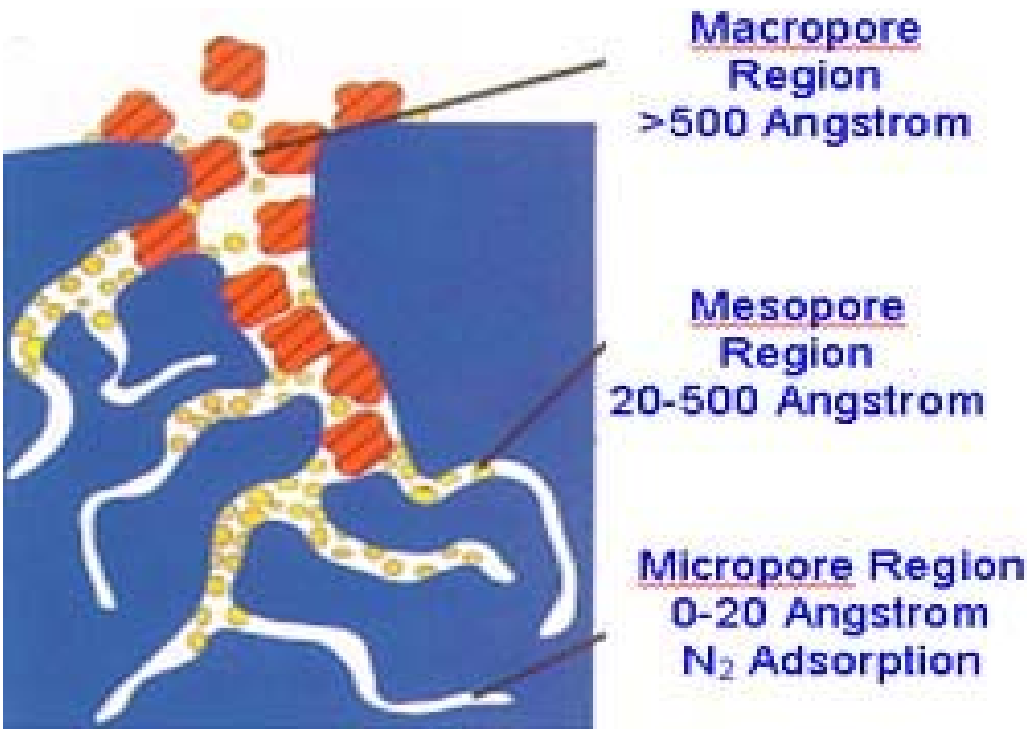

Figure 4.1 Micropore, Mesopore and Macropore Regions of Activated Carbon

Figure 4.1 shows micro, meso and macropore regions of activated carbon. In the following sections of this chapter, the main theory and methods involved in these characterization tests are given.

4.2. Adsorption Phenomena and Standard Isotherms

When a gas (adsorbate) is confined in a closed space, in the presence of an outgassed solid (adsorbent), an adsorption process begins. The gas molecules are transferred and accumulated on and in the solid material as a result of the forces between the solid surface and the adsorbate. Physical adsorption includes attractive dispersion forces and at very short distances repulsive forces as well as the contribution from the polarization and electrostatic forces between the permanent electric moment and the electric field of the solid.

The amount adsorbed on a solid surface will depend upon the temperature, pressure and the interaction potential between the vapor and the surface. Therefore, at some equilibrium pressure and temperature, a plot of weight of gas adsorbed per unit weight of adsorbent versus pressure is referred as the sorption isotherm of a particular vapor-solid interface.

Brunauer et al. (1940), based upon an extensive literature survey, found that most of the adsorption isotherms fit into one of the five types shown in Figure 4.2. Type I isotherm indicates that the pores are microporous. Type II isotherms are most frequently encountered when adsorption occurs on nonporous powders or on powders with pore diameters larger than micropores. The inflection point of the isotherm usually occurs near the completion of the first adsorbed monolayer and with increasing relative pressure, second and higher layers are completed until at saturation the number of adsorbed layers becomes infinite.

Type III isotherms are observed when the adsorbate interaction with an adsorbed layer is greater than the interaction with the adsorbent surface. Type IV isotherms occur on porous adsorbents possessing pores mainly in mesopore range. The slope increases at higher pressures as it is true for the Type II, the knee generally occurs near the completion of the first monolayer. Type V isotherms result from small adsorbate-adsorbent interaction potentials similar to the Type III isotherms. However, they are also associated with the pores in the same range as those of the Type IV isotherms. A new rare type of isotherm, Type VI recently has been found which exhibits a series of steps.

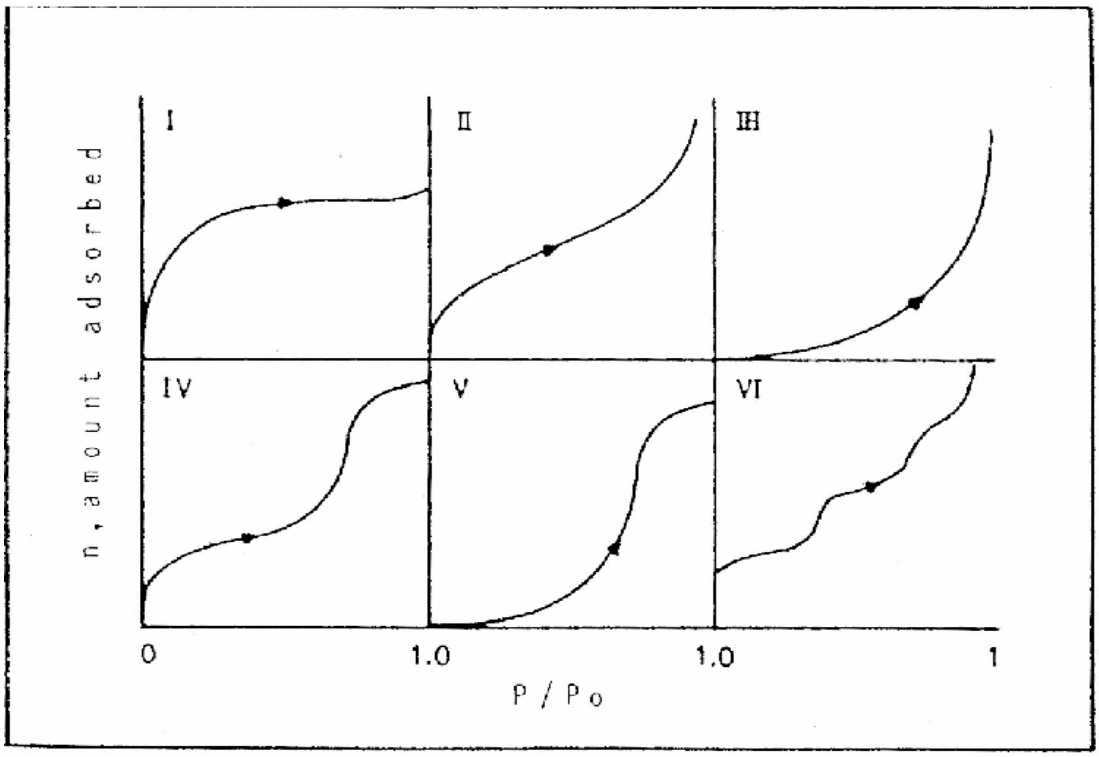

Figure 4.2 Schematic Representations of Different Types of Adsorption Isotherm

4.2.1. The Brunauer, Emmett and Teller (BET) Theory

Although derived over sixty years ago, the BET theory continues to be almost universally used because of its simplicity, and its ability to accommodate each of the five isotherm types. The BET model extends the monolayer Langmuir model to multilayer adsorption. It assumes that the surface is homogeneous and that the different layers of molecules do not interact. Each adsorbed molecule in the monolayer is assumed to be adsorption site for second layer of molecules, and so on as the relative pressure increases, until bulk condensation occurs.

In the region of relative pressures near the completion of monolayer, the BET theory and experimental isotherms do agree very well leading to a powerful and extremely useful method for the estimation of surface areas of various materials including activated carbon, coal and coal chars as well. In the final form it is given as;

$$\frac{P}{V[P_O - P]} = \frac{1}{VmC} + \frac{C-1}{V_m C}\frac{P}{P_O} \qquad (4.1)$$

where; 'V" and 'V_m" are the volume adsorbed, at the relative equilibrium pressure P/Po, and the monolayer capacity respectively, "C" is a constant, which is related exponentially to the heat of adsorption at the first and subsequent layers by the equation

$$C = \exp\left[(q_1 - q_2)/RT\right] \qquad (4.2)$$

where; "q_1" is the heat of adsorption of the first layer, "q_2", is the heat of

adsorption of the second and subsequent layers. The determination of surface areas from the BET theory is a straightforward application of equation (4.1). A plot of P/V(P-Po) versus P/Po, will yield a straight line usually in the range of 0.05 < P/Po < 0.35. The slope "S" and the intercept of "I" of a BET plot will give

$$S = \frac{[C-1]}{V_m C} \quad \text{and} \quad I = \frac{1}{V_m C} \tag{4.3}$$

Solving the preceding equations for "V_m" and "C" gives;

$$V_m = \frac{1}{S} + I \quad \text{and} \quad C = S + \frac{1}{I} \tag{4.4}$$

The BET equation usually gives a good representation of the frequently appearing Type II and IV isotherms within the range of relative pressures 0.05-0.3, and this range is generally used in practice for measurement of the surface area. At higher relative pressures, the BET equation is usually inaccurate because of capillary condensation effect, while at P/Po values below about 0.05, the amount of adsorbed gas is too small to be measured with sufficient accuracy. A poorer description is obtained for the type I, III and V isotherms, but in practice, they are often analyzed by the BET method. In order to calculate the surface area, it is necessary to know the mean cross-sectional area A_m occupied by one molecule of adsorbate gas. The specific surface area is calculated from the equation,

$$S_{BET} = \frac{V_m N_A A_m}{V_{mol}} \tag{4.5}$$

in which; "V_m" is volume of monolayer, "N_A" is the Avagadro's constant and V_{mol} is the molar volume of the gas. The cross-sectional area of any adsorbed gas molecule can be estimated from the density of the condensed phase of the gas.

For surface area determinations, nitrogen as being the ideal adsorbate, exhibits the unusual property that on almost all surfaces its "C" value is sufficiently small to prevent localized adsorption and yet adequately large to prevent the adsorbed layer from behaving as a two dimensional gas. Thus, the unique properties of nitrogen have led to its acceptance as a universal, standard adsorbate with an assigned cross sectional area of 0.162 nm^2 at its boiling point of -195.6^{o}C (Livingstone, 1949). Using BET it is possible to measure pores down to 10°A (1 nm).

4.2.2. Pore Analysis by Adsorption / Desorption

Another way to get information on the porous texture of the adsorbent is to look at the shape of the desorption isotherm. It is commonly found for porous solids that the adsorption and desorption branches are not coincident over the whole pressure range. At relative pressures above 0.3, De Boer (1958), has identified five types of hysteresis loops which is correlated with various pore shapes, Figure 4.3 shows idealization of the five types of hysteresis (Gregg and Sing, 1982).

Type I hysteresis is often associated with capillary condensation in open-ended cylindrical-shaped pores. The formation of a cylindrical meniscus occurs at a higher P/Po than the emptying process, which proceeds through the evaporation from a hemispherical meniscus. Type II corresponds to spheroidal

cavities or voids as well as to "ink- bottle" pores. The liquid trapped in the body of the pore until P/Po is reduced to allow evaporation from the neck; therefore, the release of condensate is limited by the neck radius. Type III hysteresis exhibits no limiting adsorption at P/Po = 1 is indicative of slit shaped pores. Type IV hysteresis is associated with Type I isotherms, that is with microporous adsorbents.

The hysteresis part of the isotherms contains information about the mesopores. There is a relationship between shape and position of the isotherm and the pore geometry, due to condensation and evaporation phenomena. These can be described by Kelvin's capillary condensation equation (Gregg and Sing, 1967) as;

$$r_P = \frac{-2\sigma V_{mol} Cos\ \theta}{RT \ln\left[P / P_o\right]} \tag{4.6}$$

where, "r_p" is the mean radius of the liquid meniscus, "σ" is the surface tension, "R" is the gas constant ,"T" is the absolute temperature, "(θ)" is the angle of contact between the condensed phase and the surface of the solid. In finding the pore radius by the Kelvin equation it is necessary to take into consideration the thickness "t" of the adsorbate layer. Then, the actual pore radius "r_p" is given by,

$$r_p = r_k + t \tag{4.7}$$

The term "r_k" indicates the radius into which condensation occurs at the required relative pressure. This radius, called the Kelvin radius or the critical radius, is not the actual pore radius since some adsorption has already occurred

on the pore wall prior to condensation, leaving a center core or radius, r_k. Alternatively, during desorption, an adsorbed film remains on the pore wall when evaporation of the center core takes place. Halsey (1948), set up a useful analytical expression for the thickness of the layer "t" as a function of the relative pressure,

$$t = t_m \left[\frac{5}{\ln\left(P / P_o\right)} \right]^{1/3} \tag{4.8}$$

Here, "t_m" is the thickness of the monolayer. Thus, replacing equation (4.6) and (4.8) into (4.7) for nitrogen as the adsorbate at its normal boiling point of -195.6°C, with "t_m" as 0.354 nm.

$$r_P = \frac{4.15}{\log\left(P_O / P\right)} + 3.54 \left[\frac{5}{2.303 \log\left(P_O / P\right)} \right] \tag{4.9}$$

is obtained. Here, a closely packed hexagonal liquid structure is assumed for the nitrogen molecules. The question of whether or not the adsorption or desorption branch is better suited for calculation of the mesopore size has not yet been answered definitely.

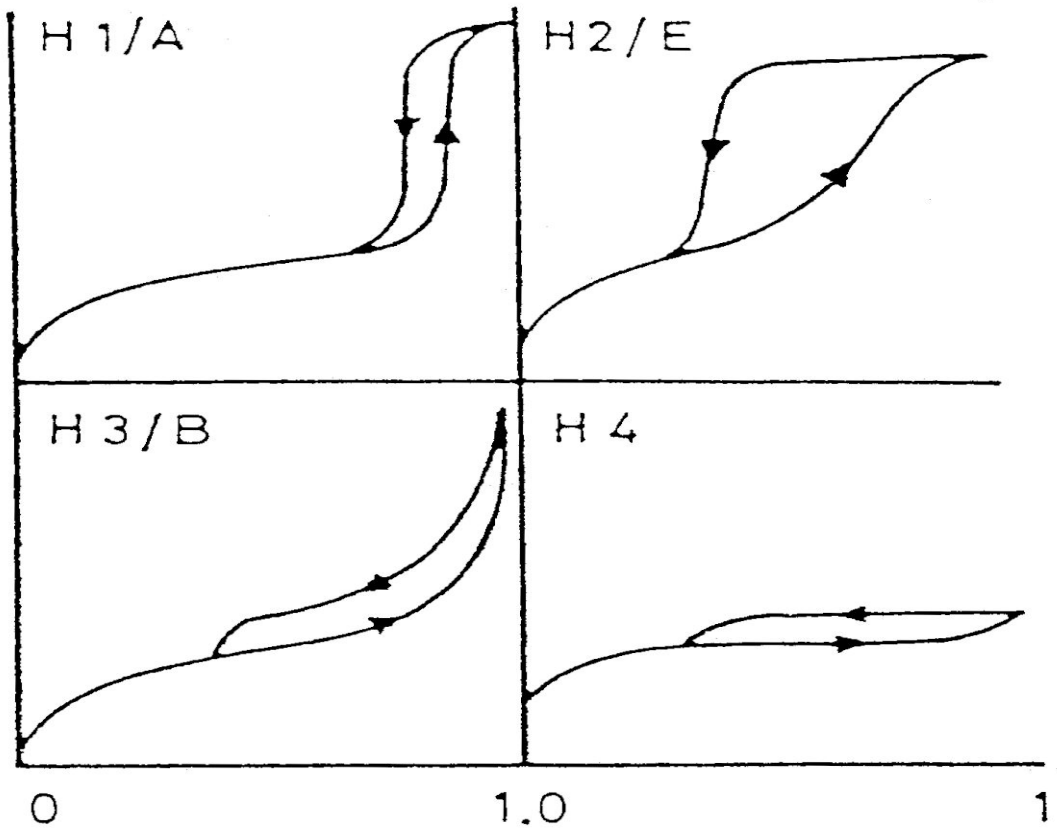

Figure 4.3 Types of Adsorption-Desorption Hysteresis Loops

For a symmetrical pore geometry, calculation of the size distribution of the mesopores from the adsorption or desorption data permits a simple determination of the mesopore surface area. The gas volumes adsorbed or desorbed upon a change of the relative pressure are taken from the isotherms, and Equation (4.9) is used to calculate the corresponding mesopore radius. Assuming certain pore geometry, the contribution to the surface area from the pores of various sizes can be found from the pore radius distribution.

Stepwise computational methods for finding the pore radius distribution and the mesopore surface area and volume are described by several investigators (Pierce, 1953; Orr, 1959; Broekhoff, 1970). One computational

method (BJH) method, proposed by Barrett, Joyner and Halenda (1951), was frequently used in practice. Derivations of the related equations are given in Appendix B. 1.

4.2.3. Characterization of Microporosity

Adsorption in microporous solids is not very well understood in comparison with non-porous or mesoporous solids. Pore sizes of similar order of magnitude as the sizes of the adsorbate molecules lead neither to the progressive completion of a monolayer nor to multilayer adsorption but to the filling up of the micropore volume with the adsorbate in a liquid like condition. A major development in understanding adsorption of gases and vapors on microporous carbons was provided by the potential theory of adsorption of Polanyi (1932).

Potential theory assumes that at the adsorbent surface the molecules of gases are compressed by attractive forces acting between the surface and the molecules and these forces of attraction decrease with increasing distance from the surface. Polanyi described the adsorption space as a series of equipotential surfaces, each with the adsorption potential E_i, and each enclosing a volume W_i. As one moves away from the surface the values of adsorption potential decrease until it falls to zero and the adsorption space increases up to a limiting value Wo (zero potential). At the surface, W=O and $E_i=E_{max}$. The building up of the volume enclosed within the adsorption space may be described by the function of the type E = f(W).

Polanyi assumed that since dispersion and electrostatic forces are independent of temperature, the adsorption potential at constant volume filling is also temperature independent. This means that the curve E = f(W) should be the same as for a given gas and a given adsorbent at all temperatures. This relationship between "E" and "*W*" is called the characteristic curve. Polanyi expressed the adsorption potential for a volume filling as the amount of work necessary to compress the adsorbate from its equilibrium vapor pressure P_1 to the compressed adsorbate pressure, P_2.

$$E = \int_{P_1}^{P_2} \frac{RT}{P} dP = RT \ln \frac{P_2}{P_1} \tag{4.10}$$

Thus, "E" is equal to the ΔG "equivalent free energy change". The state of the compressed adsorbate in the adsorption space depends on the temperature. Polanyi distinguished three different cases. (i) when the temperature is well below the critical temperature of the adsorption, T_c, adsorbed vapor may be considered as liquid like. (ii) when the temperature is just below the T_C most of the adsorbate will be as liquid like but also the adsorbate may be as compressed gas. (iii) when the temperature is above the T_c, the adsorbate will be as compressed gas. The first case is, by far, the most common one. Therefore the adsorption potential will take the form

$$E = RT \ln \frac{P_O}{P} \tag{4.11}$$

In this equation it is assumed that the liquefied adsorbate is incompressible and has the normal density of the liquid at the given adsorption temperature, then it is possible to obtain the volume filled adsorption space by

$$W = \frac{nM}{\rho} = nV_{mol} \tag{4.12}$$

where, "n" is the amount adsorbed in moles, "M" is the molecular weight of the adsorbate and "ρ" is the liquid density. The temperature-invariance of the adsorption potential which is the fundamental postulate of the Polanyi's theory, has been demonstrated, mainly by Dubinin and co-workers (1966) and they have added a second postulate. They stated that for an identical degree of filling of the volume of adsorption space, the ratio of adsorption potentials for any two vapors is constant which is called the affinity coefficient, *"β".* Dubinin's treatment has been modified by Kaganer to yield a method for calculation of specific surface from the isotherm. Using the experimental data and assuming that pore size distribution is Gaussian, Dubinin and Radushkevich, 1947, arrived at an expression which is known as "Dubinin Radushkevich", (D-R) equation;

$$\log W = \log W_O - D \log^2 \left(\frac{P_O}{P} \right) \tag{4.13}$$

where D is 2.303 K (RT / β)^2. A plot of log W against log (Po/P) will be straight line having an intercept equal to micropore volume, "W_o". Dubinin and Astakhov (1971), assuming a Weibull distribution of pore sizes, rather than a Gaussian, obtained the following "Dubinin - Astakhov, (D-A)" equation;

$$\log W = \log W_O - D' \log^n \left(\frac{P_O}{P} \right) \tag{4.14}$$

where D'= $2.303^{(n-1)}$ $(RT/E)^n$. It follows from the equation (4.14), that "DR" equation is a special case of "D-A" equation (4.13), when n=2. The lower limit of CO_2 adsorption technique is down to 4-5°A.

4.3. Mercury Intrusion Porosimetry

Washburn in 1921 first suggested the use of Mercury intrusion under pressure to determine the pore size distribution of porous solids. The principle of the mercury intrusion technique is based on forcing the mercury under increasing pressure into successively smaller pores.

An important feature of mercury utilized in this technique is that it exhibits a contact angle of greater than 90° with most materials. This means that mercury will neither penetrate the openings of particles nor pore space within the material unless forced. The volume of mercury penetrated into the solid is measured as a function of the applied pressure which is related by the Washburn equation as,

$$rp = \frac{-2\gamma Cos \theta}{P} \tag{4.15}$$

where; " r_p" is the radius of circular pore, "γ" is the surface tension of mercury in the pore, 'θ 'is the angle of wetting of the pore wall by mercury "P" is the total pressure exerted under which mercury is made to penetrate the pores. From this, the pore volume and pore surface area distributions can be calculated. The lower limit of this technique is down to 60°A. Derivation of the above equation is given in Appendix A.1.

4.4. Density and Total Pore Volume Determinations

The total pore volume and porosity of activated carbon can be determined by using the combination of apparent and true density measurements.

True density of a porous solid is defined as the ratio of the mass to the volume occupied by that mass. Therefore, contribution to the volume made by pores or internal voids must be excluded when measuring the true density. To determine the true density of a solid, one needs to have a non interacting fluid which completely fills all the pores. In reality, no fluid completely fills the pore volume of activated carbons. Therefore, the term, true density should be treated in this way.

Helium is the smallest molecule available with an atomic diameter of 1.7°A. Therefore, it has the best chance of penetrating the entire porosity of activated carbon. Apparent density is defined as the weight of the solid divided by the volume including the internal pores of that solid. Apparent density measurement is most commonly determined from the volume of mercury displaced under pressure to fill the interparticle (interstitial space) void volume only. Then, total pore volume and total porosity of the activated carbon can be evaluated as

$$\text{Total pore volume (cm}^3\text{/g)} = \frac{1}{\rho_{Hg}} - \frac{1}{\rho_{He}} \tag{4.16}$$

$$\text{Total porosity} = 1 - \frac{\rho_{Hg}}{\rho_{He}} \tag{4.17}$$

Figure 4.4 depicts a block-diagram of the overall experimental approach. The physical characterization of activated carbon samples were characterized according to this scheme (Şenel, 1994).

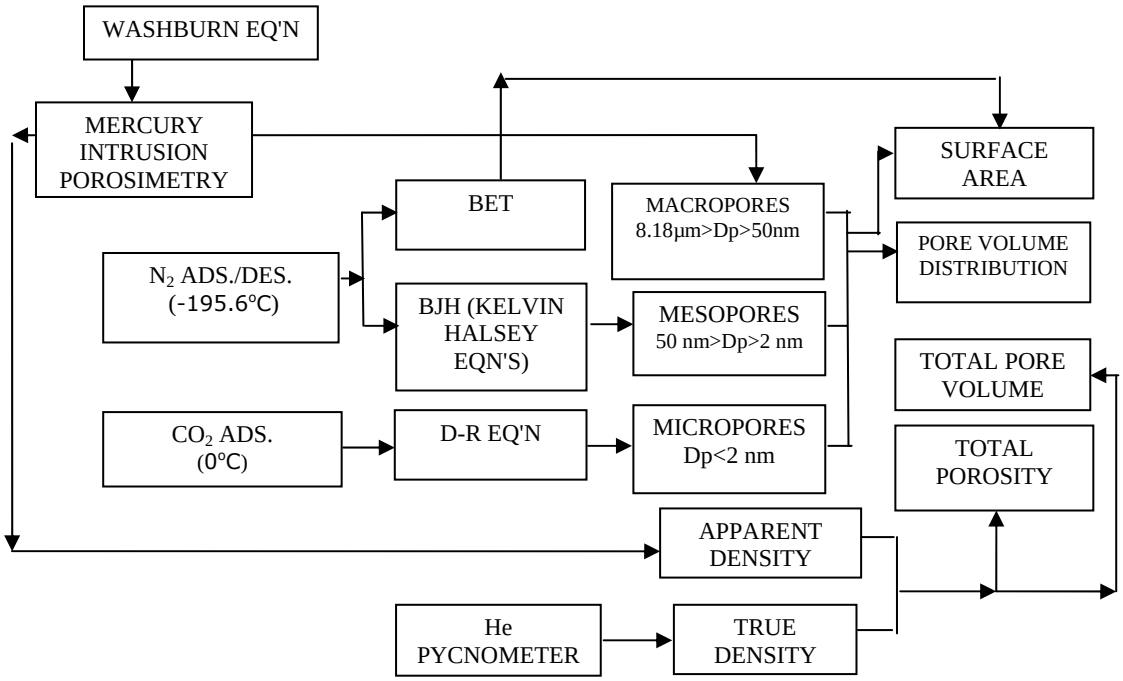

Figure 4.4 Block-Diagram of the Overall Experimental Approach (Şenel, 1994)

CHAPTER V

EXPERIMENTAL WORK

The main aim of this study was, to produce activated carbon from an agricultural waste; apricot stones and to characterize this activated carbon. To produce activated carbon, at the selected conditions, chemical activation method was applied to apricot stones.

5.1. Properties and Preparation of Apricot Stones

5.1.1. Properties of Apricot Stones

Apricot stones used throughout the experiments were obtained from a garden in Malatya.

Elemental analysis of apricot stone and activated carbons were determined using a "Leco CHN Elemental Analyzer". Ash content of them was determined by following TS 6879 (Turkish Standards Institution (TSE)). Chemical composition of apricot stones is given in Table 5.1.

Table 5.1 Chemical Composition of Apricot Stones

C %(wt)	H %(wt)	N %(wt)	O (by difference) %(wt)	Ash %(wt)
50.41	5.66	Trace	43.661	0.269

5.1.2. Preparation of Apricot Stones

As stated in Section 3.2.2. in the activated carbon production, in this study, chemical activation technique (activation after chemical agent impregnation to raw material) was used. To prepare the raw material (apricot stones) the procedure given below was applied.

First the apricot stones were dried at room temperature then crushed with hammer. The resulting particles were sieved and the particles having sizes between 10- 18 mesh (1-2 mm) were used in the rest of the experimental work. For phosphoric acid (H_3PO_4) impregnated samples, apricot stones were treated with the 50% (vol) H_3PO_4 solution at 25°C at ratio of 2.66:1 (weight) for 24 hours. This corresponds to, 1 g apricot stone impregnated with 2 ml %50vol phosphoric acid (H_3PO_4).

After impregnation, solution was filtered to take the residual acid. Subsequently impregnated samples were air dried at room temperature for 3 days. Impregnated apricot stones samples containing %18 H_3PO_4 were obtained after dried. Since the impregnation ratio is the most important factor effecting pore size distribution, in chemical activation technique, several initial experiments were done to obtain the best impregnation method.

For this purpose three different methods were applied. First, impregnated samples were filtered and dried after washing with distilled water. Second, impregnated samples filtered and dried at 60°C in an oven. Lastly, impregnated samples were filtered and dried at room temperature (25°C). Three AC3.1 experiments were done using these samples.

The best BET surface area value of 444m^2/g was obtained from the third sample that impregnated, filtered and dried at room temperature for three days. In the rest of the experimental work third method of impregnation was used. The BET surface areas of first, second and third type of impregnation measured were 4, 120 and 444m^2/g, respectively. With third impregnation method the impregnation ratio obtained of 18%. In another words, 18 g phosphoric acid was impregnated into the 100 g raw apricot stone sample. After all of these procedures the samples were ready for the carbonization experiments.

5.2. Carbonization Experiments

5.2.1. Experimental Set-Up

Carbonization experiments were carried out in a horizontal "Lenton Unit C2" furnace. To ensure the inert atmosphere in the furnace by N_2 gas flow, 20 mm inside (24 mm outside) diameter quartz tube length of 90 cm was placed horizontally into the furnace. The inlet and the outlet of quartz tube connected with quartz fittings, to avoid the escape of N_2 from the system and to avoid the entrance of air to the system.

To measure the N_2 flow rate passing through the system a N_2 flow meter connected to inlet of furnace. A bubbler in a cooling bath was used at the outlet of the system to cool the outlet gases and to show the N_2 flow by bubbling. After cooling, the outlet gases purged to hood by a heat resistant hose. Experimental set up used in the experiments is shown in Figure 5.1.

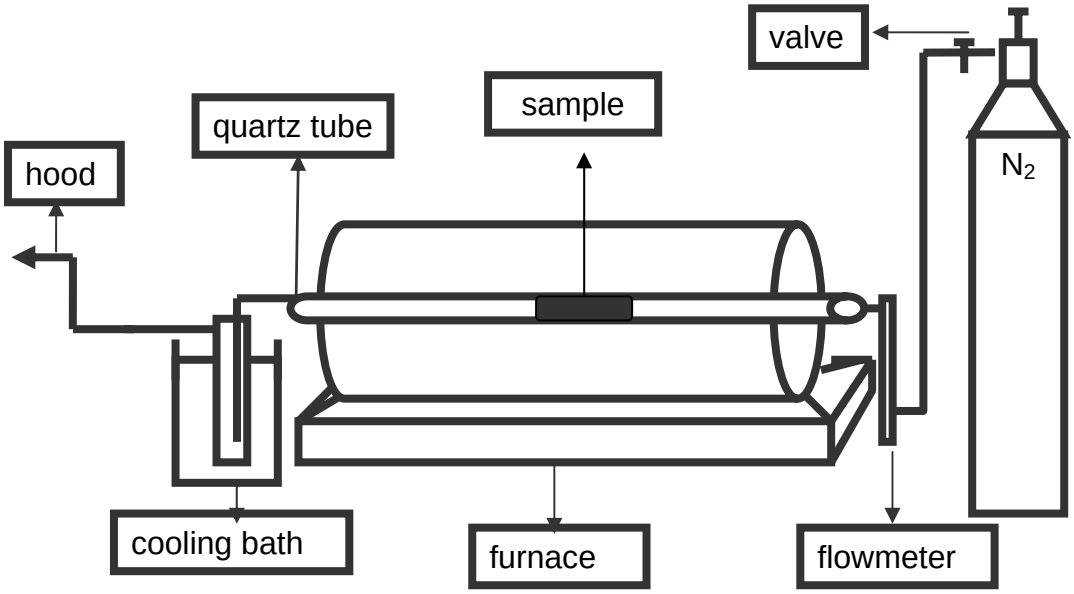

Figure 5.1 Experimental Set-Up

5.2.2. Chemical Activation of Samples

Activation of phosphoric acid impregnated raw material was carried out by carbonizing that material under nitrogen flow (180cm^3/g) at a heating rate of 20°C/min. The furnace has temperature programming heating rate. For each experiment 20 g of impregnated sample used. Yields of each experiment are shown in Section 6.3. Experiments were repeated at different final carbonization temperatures 300°C, 400°C and 500°C. Carbonization times were 90, 120, 180 and 210 minutes at each temperature. Samples were placed in furnace then N_2 flow started to purge the air in the quartz tube for 30 minutes. After purging

furnace was started to heat till chosen carbonization temperature achieved, and temperature was kept constant by the temperature controller of furnace. Carbonization time started when temperature reached and held at the final carbonization temperature. As carbonization time is reached, furnace was started to cooling using a hair dryer. Lastly, when the temperature of furnace decreased down to 100°C product was taken to a flask and distilled water was added to prevent interaction with the air. The procedure followed in experiments is shown in Figure 5.2. as a scheme. Experimental conditions and samples codes are given in Table 5.2.

Table 5.2 Experimental Conditions and Samples Codes

Experimental Constants		Experimental Variables		
Particle Size	1-2 mm	Carbonization Temp.(°C)	Carbonization Time(min)	Sample Codes
N_2 Flow Rate	180 cm^3/g	300°C	90	AC 3.1
			120	AC 3.2
			180	AC 3.3
			210	AC 3.4
Heating Rate	20°C/min	400°C	90	AC 4.1
			120	AC 4.2
			180	AC 4.3
			210	AC 4.4
Acid / Stones Ratio	2.66/1 (weight)	500°C	90	AC 5.1
			120	AC 5.2
			180	AC 5.3
			210	AC 5.4

5.3. Characterization of the Products

Before the characterization, products were crushed to obtain small particles (30-70 mesh or 0.595-0.212 mm) and rinsed with boiling distilled water to decrease the pH value of the activated carbon to 4. Initial experiments showed that surface area of the products crushed after the carbonization was higher than the products not crushed. The tarry substances produced during carbonization can not be evacuated from the opened pores using boiled distilled water. And if the products are not crushed, it is difficult to dissolve these tarry substances with boiling distilled water.

These tarry substances also increase the pH value of the products which in turn seemed to affect the surface area of the activated carbon. pH values of the activated carbons were determined by following TS 5896 (Turkish Standards Institution (TSE)). Procedure followed in experiments is shown in Figure 5.2. The products produced by the procedure given in Figure 5.2 are granular activated carbons (GACs) with the particle sizes of 30-70 mesh.

Prior to making all characterization tests, the samples were first oven dried at 113°C for 10 hours under vacuum. For the characterization of the products, pore structure variation with carbonization temperature and time, total surface area and solid densities were examined.

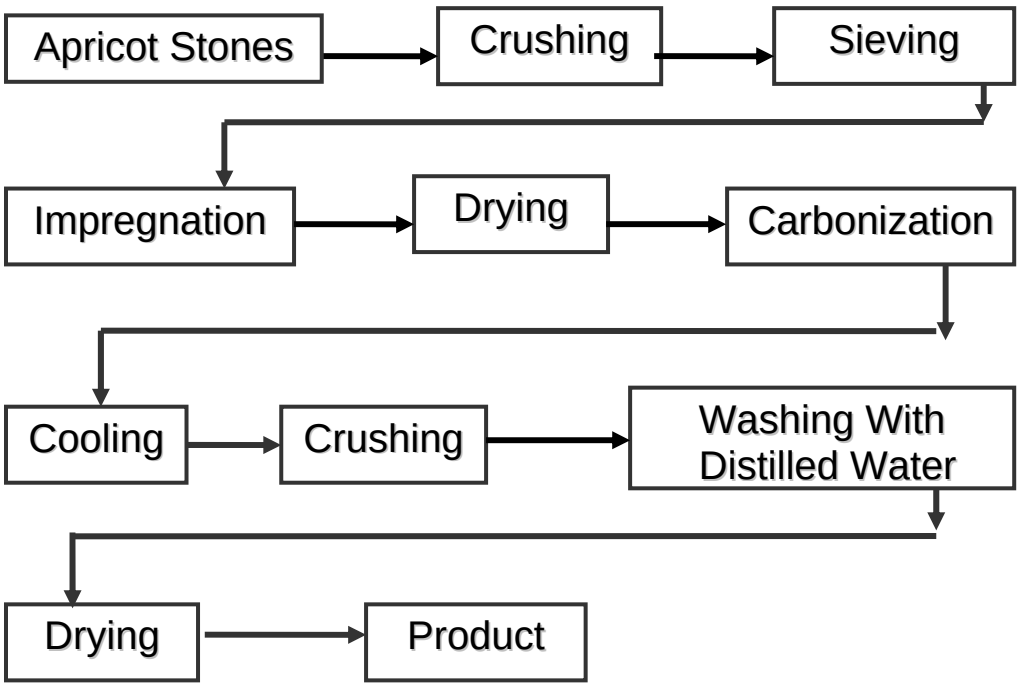

Figure 5.2 Procedure Followed in Experiments

5.3.1. Nitrogen Gas Adsorption Measurements

A commercial volumetric gas adsorption apparatus "ASAP 2000", Accelerated Surface Area and Porosimetry System manufactured by Micromeritics Co., USA was used to measure the surface area and to determine the pore size distributions of mesopores using N_2 adsorption data at -195.6°C. Analysis of the micropores was also determined by this unit by CO_2 adsorption at 0°C, the details of which are explained in the following section. Schematic diagram of this apparatus is given in Figure 5.3.

To measure the mesopore surface area and the mesopore volume of the samples nitrogen gas adsorption and desorption isotherms were obtained at -195.6°C. For each experimental point, an equilibration time of about 30 minutes was allowed. The cross sectional area of the nitrogen molecule was taken as

0.162 nm^2 (Walker et al., 1968). Surface area of the samples was determined by using BET equation in the relative pressure range of between 0.05 to 0.999 over twenty adsorption points. The area and the volumes of the pores as well as their distributions were evaluated from the nitrogen adsorption isotherms using the Barrett, Joyner and Halenda (BJH) method (as indicated in section 4.2.2), (Barrett et al., 1951) considering the IUPAC mesopore range definition which ranges from 50 nm down to 2 nm in terms of the pore diameters of the cylindrical shaped pores.

5.3.2. CO_2 Gas Adsorption Measurements

The micropore volume of the samples was estimated by application of the Dubinin-Radushkevich equation to carbon dioxide adsorption at 0^oC.

The data were automatically collected and evaluated by using the software/ computer system. At least half an hour were allowed for equilibrium to be established at each point of the CO_2 isotherm. Micropore surface area of the samples were calculated from the DR micropore volume, taking the cross sectional area and the density of a CO_2 molecule as 0.17 nm^2 (Micromeritics ASAP 2000, User Manual, Appendix C, 1993) and 1.181 g/cm^3 (Micromeritics ASAP 2000, User Manual, Appendix C, 1993), respectively. The saturation vapor pressure was taken as 26142.000 mm Hg at the analysis temperature of 0^oC (Micromeritics ASAP 2000, User Manual, Appendix C, 1993).

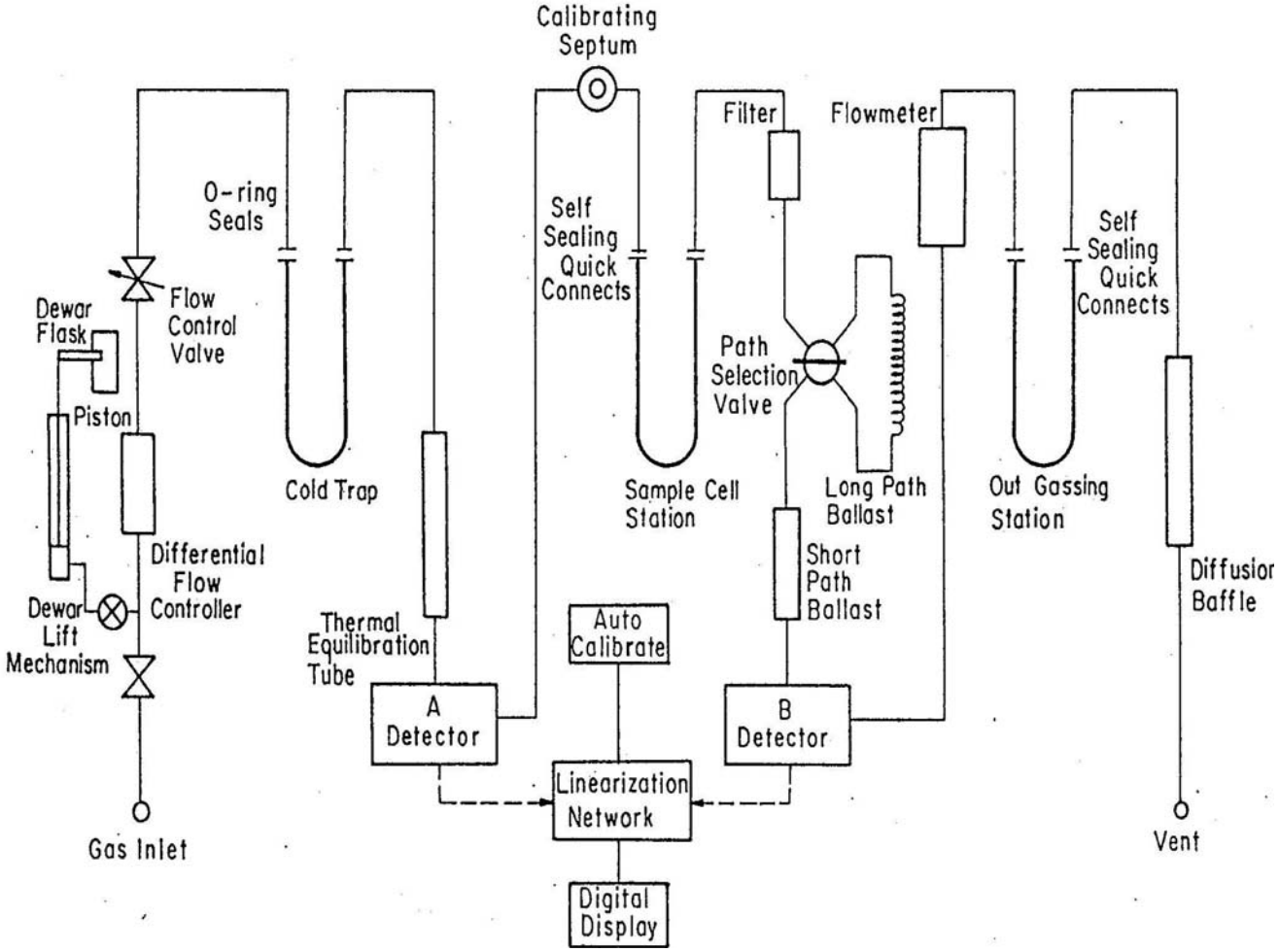

Figure 5.3 Schematic Representation of Surface Analyzer

5.3.3. Mercury Porosimetry

Pore volume, area and the distributions of the pores in the macropores region as well as the apparent density data of the samples were determined by using a commercial automated high pressure mercury intrusion porosimeter (Micromeritics Poresizer 9310, Micromeritics Inst. Co., USA).

About 0.25-0.3 g of sample was weighed and placed into a glass penetrometer. After weighing, penetrometer was assembled to the low pressure manifold and degassing until a sufficient vacuum level was attained (less than 30 μm Hg). Then, triply distillated mercury was introduced into the penetrometer until penetrometer was filled. Pressure was gradually increased to 22 psi with the increments of 2 psi for the low pressure port of the test (up to 22psi). Mercury filled penetrometer was weighed and replaced to the high pressure compartment and pressure was stepwise increased to a final pressure of 27000 psi. Sufficient equilibration time was allowed for each intrusion points. Thus, a complete analysis lasted 2 to 3 hours for taking about 30 intrusion points. Pores which are in the pressure range of 22 psia (d_{pore}=8180 nm) to 3600 psia (d_{pore}=50 nm) can be considered as macropores, by applying the Washburn equation (eqn. 4.15) and considering the IUPAC definition. Apparent density values were calculated from the measurements of mercury displaced by the samples at 22 psia since, in the determination of apparent density, in interparticle voids should be excluded while internal pores should be included.

5.3.4. True Density and Total Pore Volume Determinations

True (Helium) density of samples were determined by using a commercial pycnometer, "The Multivolume Pycnometer, Model 1305" manufactured by Micromeritics. Schematic diagram of this apparatus is given in Figure 5.4. The He Pycnometer instrument is consisted essentially of a sample-holding vessel, a cylinder fitted with a movable piston, the relative position of which is indicated on the front panel dial to five decimal places and a pressure detector. A dial light reveals whether the pressure in the system is the same as that in the detector.

In a typical run, 0.1-0.2 g degassed sample was placed into a propylene cup and then, both were evacuated in the pycnometer chamber for a sufficient time. After filling the system with helium, chamber was opened to atmosphere by means of a 4 position valve. By this way, enough helium is allowed to escape into the system in order to reduce pressure in the system to the atmospheric reference pressure.

After some time, the valve was turned to gauge position for sealing the helium in the system at atmospheric reference pressure. Once the valve in gauge position, the variable volume chamber, sample chamber and pressure detector are connected and sealed off as a closed system. When the variable volume is changed so as to decrease the volume of the system, the pressure increase to the point where contact is broken between the bellows of the pressure detector and an electric contact in the detector. This indicates where the reading should be taken. After obtaining three values; for empty cup, for standard volume and for sample as "V_{CELL}", "V_{EXP}" and "V_{SAMP}" values,

respectively, true density of the sample was determined using the known weight of sample according to procedure given in Appendix D. Total pore volumes and total porosities were then calculated combining the true and apparent density values by means of the equations 4.16 and 4.17, respectively.

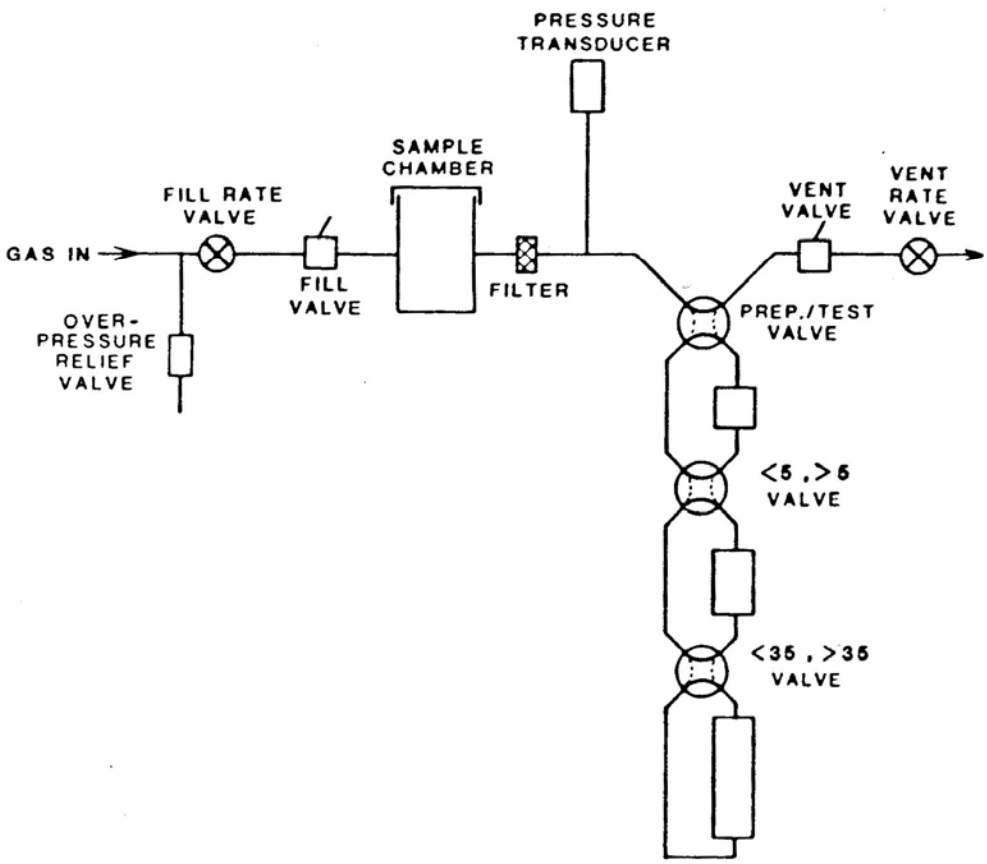

Figure 5.4 Schematic Diagram of Helium Pycnometry

CHAPTER VI

RESULTS AND DISCUSSION

Activated carbon production from apricot stones has been achieved by the chemical activation technique using phosphoric acid as activating agent. By changing carbonization time and carbonization temperature twelve activated carbon products have been produced.

One of the major objectives of this study was to investigate the pore structure of activated carbon produced from apricot stones at relatively low temperatures (300, 400 and 500°C). The pore structure of the activated carbon was characterized by different physical techniques; nitrogen adsorption at -195.6^{o}C, carbon dioxide adsorption at 0°C, mercury porosimetry and helium pycnometry.

In terms of chemical characterization, the analyses were limited to determination of C, H, N, O elements and ash analysis; to provide information with respect to elemental composition. Under identical experimental conditions,

TGA experiments were carried out to supply information in terms of yields of acid impregnated and raw apricot stones.

6.1. Chemical Analysis of Products

Elemental (C, H, O) analysis of these twelve activated carbons which was carried out according to the procedure explained in section 5.1.1. is given in Figure 6.1 and Table E.1. As it can seen from this figure, activated carbons produced in this study contain about 66.2-84.7 % carbon, 1.8-4.1 % H , 7.2-25.8 % oxygen, trace amount of N and 3.2-7.7 % ash.

6.1.1. Carbon Content

Data reported in Figure 6.1. indicates that, carbon content of the AC3 series (carbonization temperature of 300°C) and AC5 series (carbonization temperature of 500°C) increasing for first three carbonization times 90, 120 and 180 min, respectively and decreasing for the longest carbonization time of 210 minutes.

However, carbon content of the AC4 series (carbonization temperature of 400°C) remaining constant for the first two carbonization times, 90 and 120 min. respectively and decreasing and remaining constant for the last two times, 180 and 210 min. respectively.

The highest carbon content of 84.7 % is obtained from AC 4.1 and AC 4.2 samples. For a typical activated carbon, carbon content is reported to be around 85-90 % (Section 3.4, Faust and Aly, 1983). As carbon content of the

activated carbon increase it is expected that the BET surface area value increase. BET area value is the most important parameter for activated carbons. High carbon content value is desired to achieve high BET surface area.

6.1.2. Oxygen and Hydrogen Content

The presence of oxygen and hydrogen influence the adsorptive properties of activated carbon. As discussed in Section 3.4.1 and 3.4.2 these elements are combined with the atoms of carbon by chemical bonds. The oxygen hydrogen functional groups provide sites where molecules of water and other polar substances or easily polarizable gases and vapors are adsorbed (Smisek and Cerny, 1970; Hassler, 1971).

However, O and H contents of the samples are slightly higher than typical values. For AC3, AC4 and AC5 series oxygen content values are in the range of 14-25%, 8-15% and 7-18%, respectively. O content of AC3 series is higher than AC4 and AC5 series. H contents of AC3, AC4 and AC5 series are in the range of 2.8-4.1%, 2.4-3.5% and 1.8-2.9%, respectively. As carbonization temperature increases H contents of the products decrease. The lowest values are obtained from AC5 series. Because of phosphoric acid (H_3PO_4) used as activating agent and it contains hydrogen and oxygen groups in structure, these high O and H content values could be obtained. Since pH values of the all samples are 4, it is expected that H^+ concentrations of samples are at high values. This increases the H contents of the samples. For a typical activated carbon the recommended oxygen content is around 5 % and the hydrogen content is 1 % (Faust and Aly, 1983).

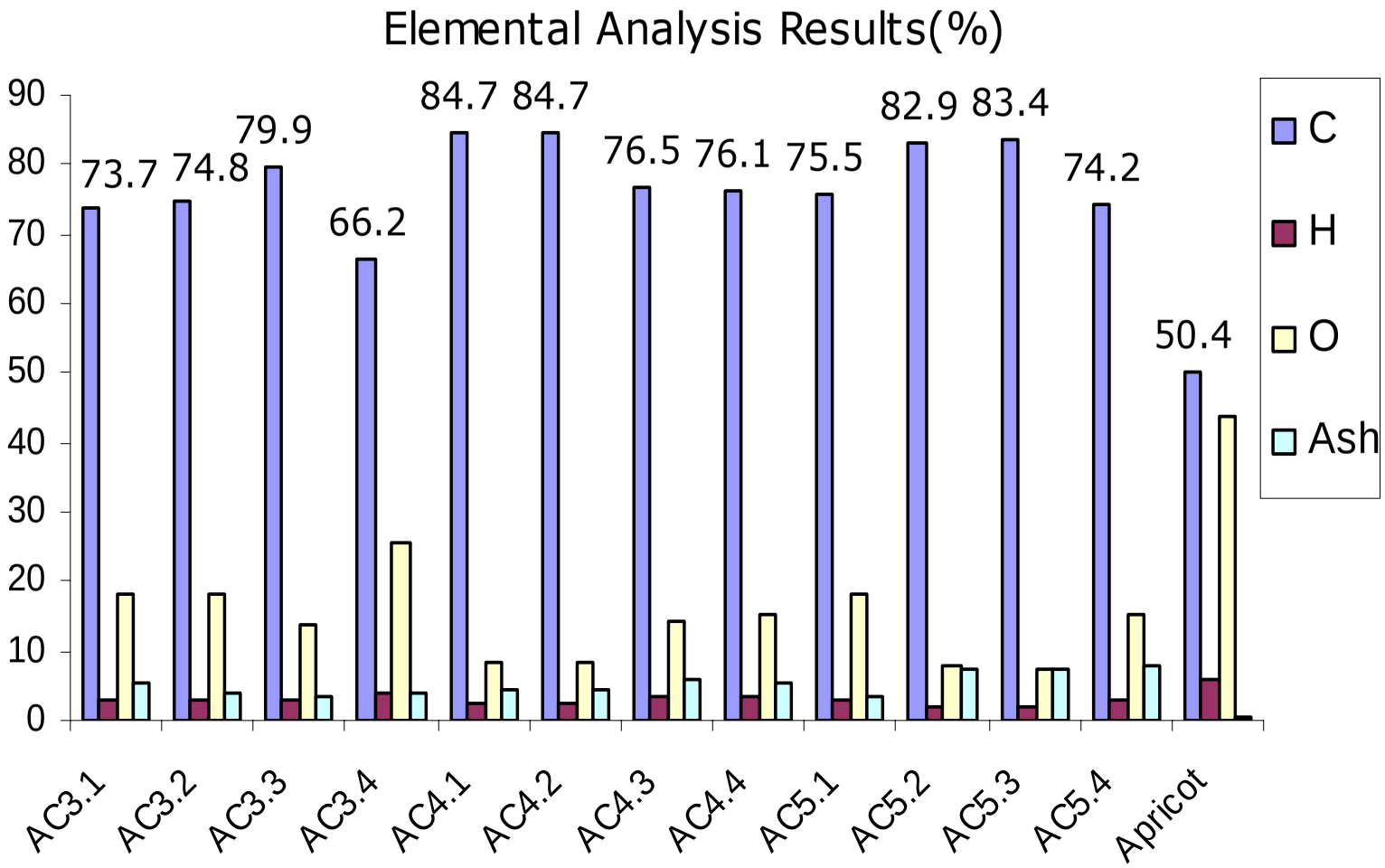

Figure 6.1 Chemical Compositions of Activated Carbons

6.1.3. Nitrogen Content

For a typical activated carbon, nitrogen content is less than 1 %. All the products obtained from apricot stones by chemical activation have nitrogen contents in small amounts which are less than 1 percent (Figure 6.1.). During carbonization in nitrogen atmosphere, small amount of nitrogen can be chemisorped (Smisek and Cerny, 1970;).

6.1.4. Ash content

A good activated carbon must have low ash content. A small increase in ash content causes a decrease in adsorptive properties of activated carbon. The raw material, apricot stones have ash content about of 0.27% (Table 5.2).

However, ash content of the samples is slightly higher than typical values. For AC3, AC4 and AC5 series these values are in the range of 3.2-5.4%, 4.5-5.8% and 3.2-7.7%, respectively. Especially ash content of AC5 series is higher than AC3 and AC4 series. As carbonization temperature increases ash contents of the samples increase. These results may be caused by high heating rate and impregnation ratio. As indicated in Section 2.1 depolymerization reactions between the volatile materials and phosphoric acid during the carbonization were affected. Although phosphoric acid (H_3PO_4) restricts the formation of tar, high heating rate (as indicated in Section 2.1) and high impregnation ratio increase the formation of tar so, it is expected that as tar formation increases ash content of the samples increases.

To decrease these values some experimental parameters which was taken constant during experiments such as heating rate and impregnation ratio values could be reduced.

6.2. Physical Characterization of the Products

The physical characterization of the twelve activated carbons was carried out according to the experimental procedures given in Figure 4.4. The samples were characterized by determination of their pore size distribution, total pore volume, apparent and solid density, mesopore area, micropore area, macropore area, macropore volume, mesopore volume, micropore volume and surface area. Mercury intrusion porosimetry, BET (N_2) surface area measurement, Helium pycnometry and D-R method (CO_2) are used to determine these values.

6.2.1. Nitrogen Gas Adsorption Measurements

The nitrogen adsorption measurements of the twelve samples include the determination of the (i) BET surface area, "S_{BET}", (ii) volume of mesopores, "V_{MESO}", and (iii) cumulative surface area of mesopores, "S_{MESO}".

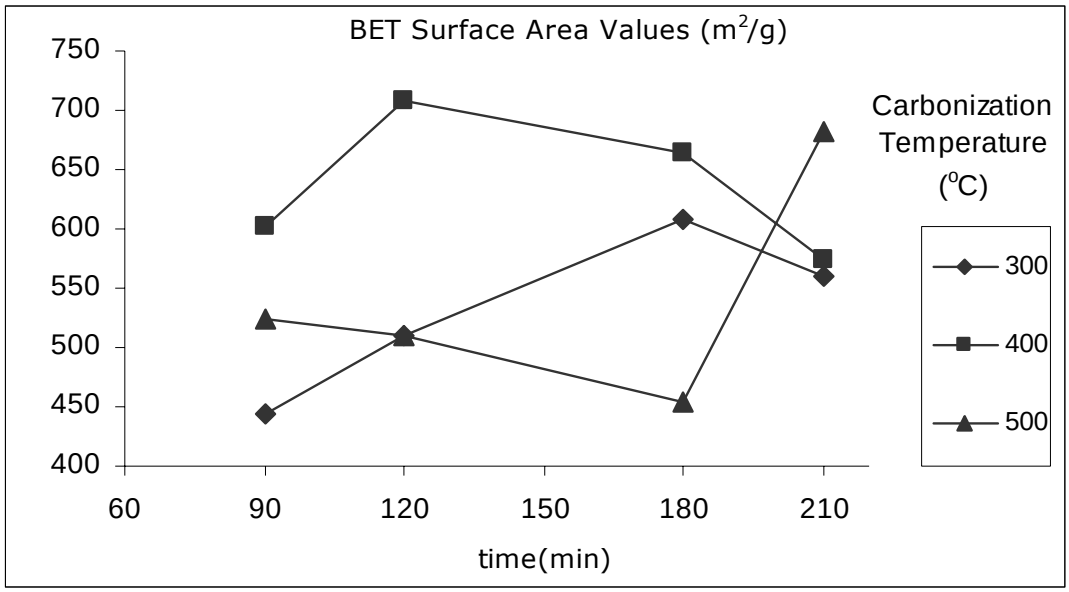

Figure 6.2 BET Surface Areas of the Samples

BET surface area values of the samples are shown in the Figure 6.2. Sample AC4.2 had the highest BET area, 709 m^2/g and sample AC3.1 had the lowest BET area 444 m^2/g. AC3 and AC4 series values gave a maximum while AC5 series values gave a minimum. The BET areas of the samples are close to literature values. BET areas of the commercial activated carbons are in the range of 600-1500 m^2/g. The reproducibility of the experiments was checked by characterizing repeated runs using BET, and the results were found to be almost the same.

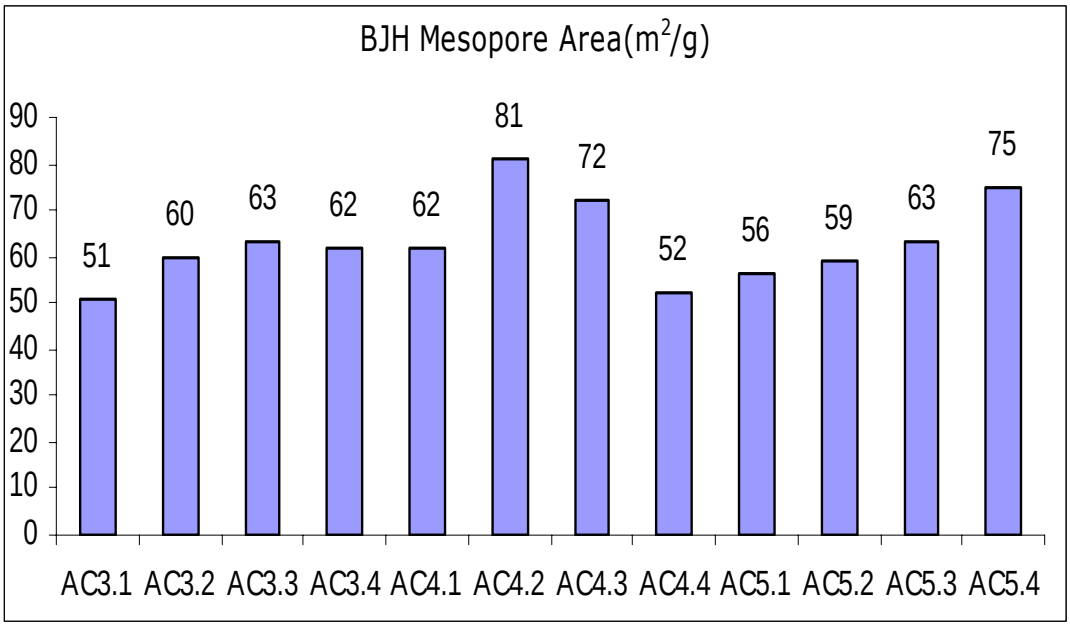

Figure 6.3 BJH Meseopore Areas of the Samples

Mesopore area of the samples are in the range of 51 to 81 m^2/g. For all samples mesopore areas are around 10-12 % of the BET surface areas. It is shown from the values of AC5.1, AC5.2 and AC5.3 mesopore area increasing with the increasing carbonization time while BET area values decreasing. It means as carbonization time increase the pores are getting wider. Mesopore surface area values of the samples are high enough to allow its usage in liquid phase processes such as sugar discolourization.

As it is shown in the Figure 6.4 mesopore volumes of the samples are in the range of 0.03-0.05 cm^3/g. Mesopore volume values are directly related with the mesopore area values.

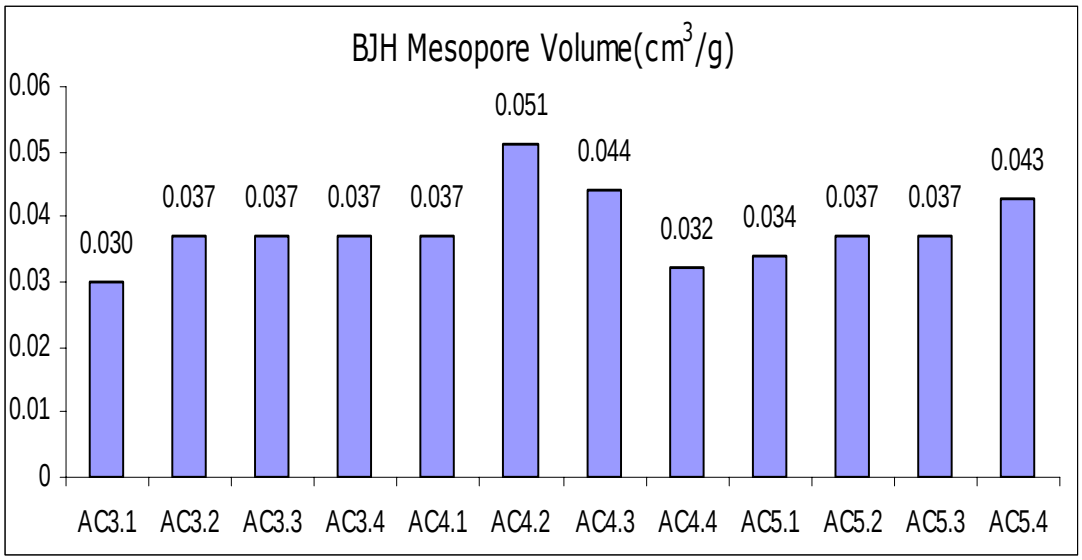

Figure 6.4 Mesopore Volumes of the Samples

Isotherm shapes in the literature which were originally defined by Brunauer et al. (1943) and classified into 6 well-known groups, (as it is shown in Figure 4.2) one may say that almost all products show similar isotherms to the type I. According to Brunauer, this type of isotherm is observed in the case of microporous solids.

As discussed in section 4.2.2, another way of obtaining information on the porous texture of the solids is to compare the shape of the hysteresis loop (Figure 4.3) with the shape of adsorption and desorption branches of the standard shapes which were originally classified by De Boer (1958). But, as it is shown in the isotherm figures of the samples, there is no distinct hysteresis loops at adsorption / desorption isotherms.

Figures 6.5, 6.6 and 6.7 show the N_2 adsorption / desorption isotherms of the samples.

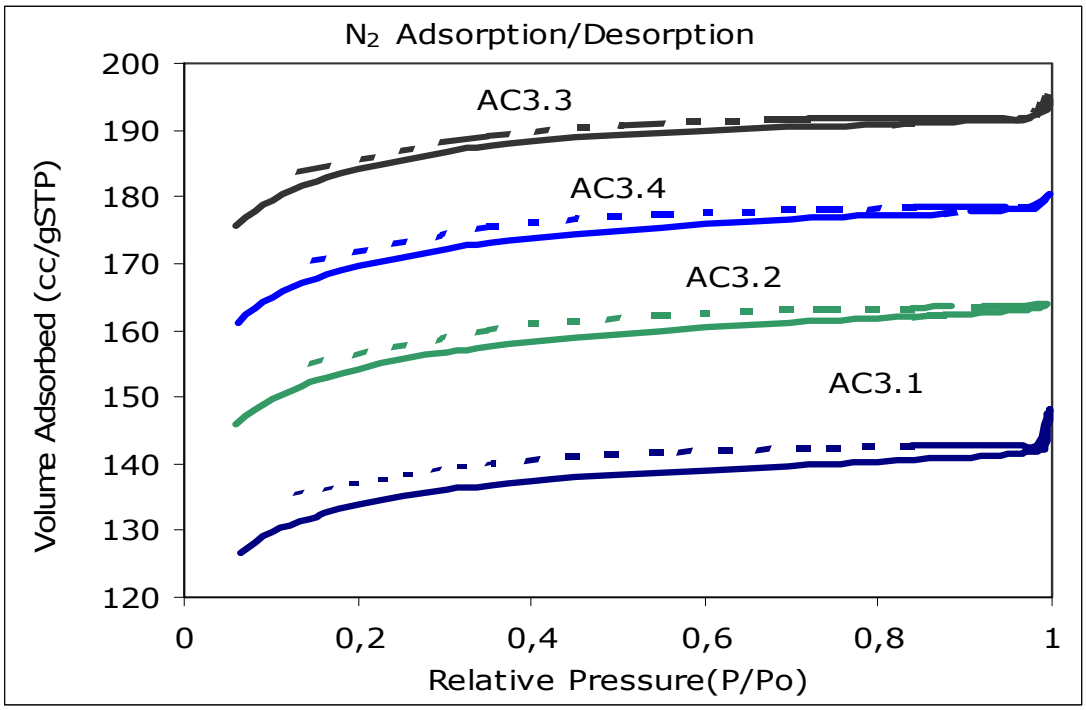

Figure 6.5 N_2 Adsorption/Desorption Isotherms of AC3 Series

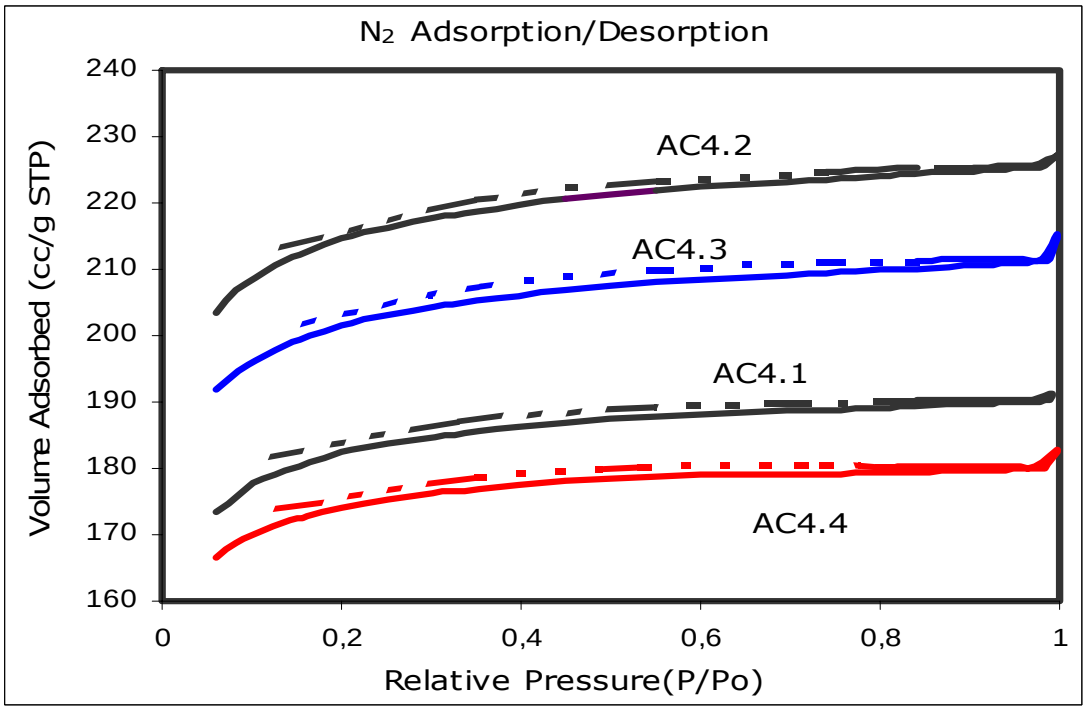

Figure 6.6 N_2 Adsorption/Desorption Isotherms of AC4 Series

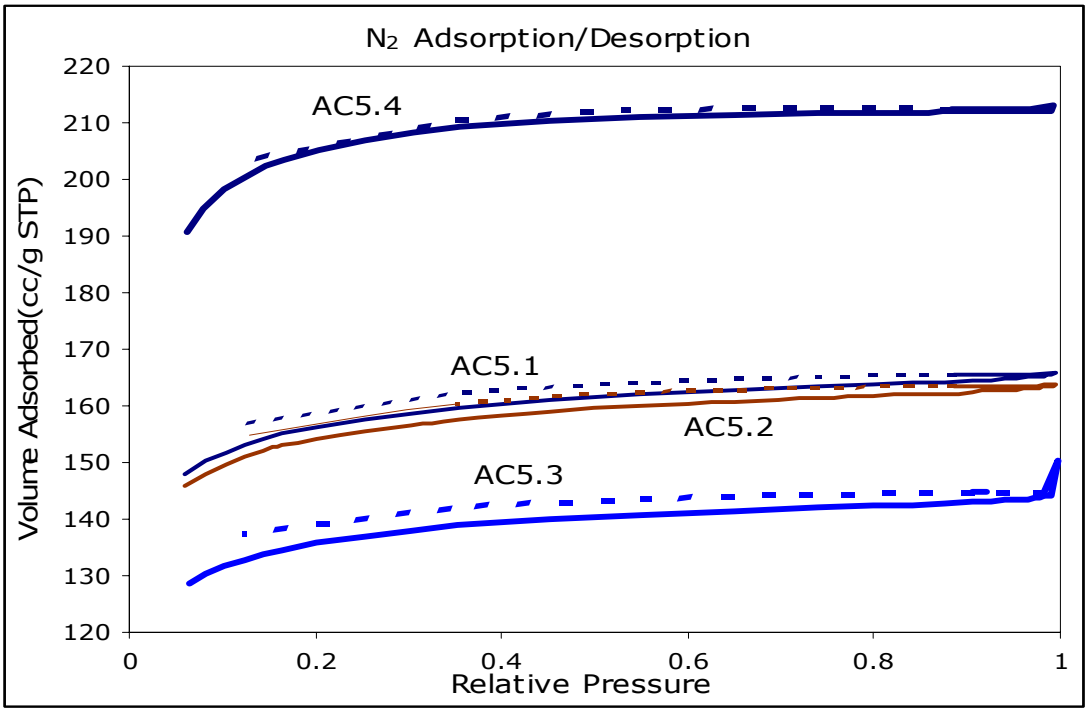

Figure 6.7 N_2 Adsorption/Desorption Isotherms of AC5 Series

6.2.2. Carbon Dioxide Gas Adsorption Measurements

Micropore analysis of the samples was carried out by CO_2 adsorption studies as described in section 5.3.2. This method was applied because CO_2 adsorption at 0°C is widely used in literature for reporting the micropore volume and the surface area of the activated carbons.

For this purpose, the micropore volumes were calculated from intercept of the volume of CO_2 adsorbed, versus $(P/P_o)^2$ in log-log plot, using the Dubinin-Radushkevich (D-R) equation. The relative pressures, P/P_o employed in all measurements were in the range of 1.10^{-4} to 1.10^{-2}.

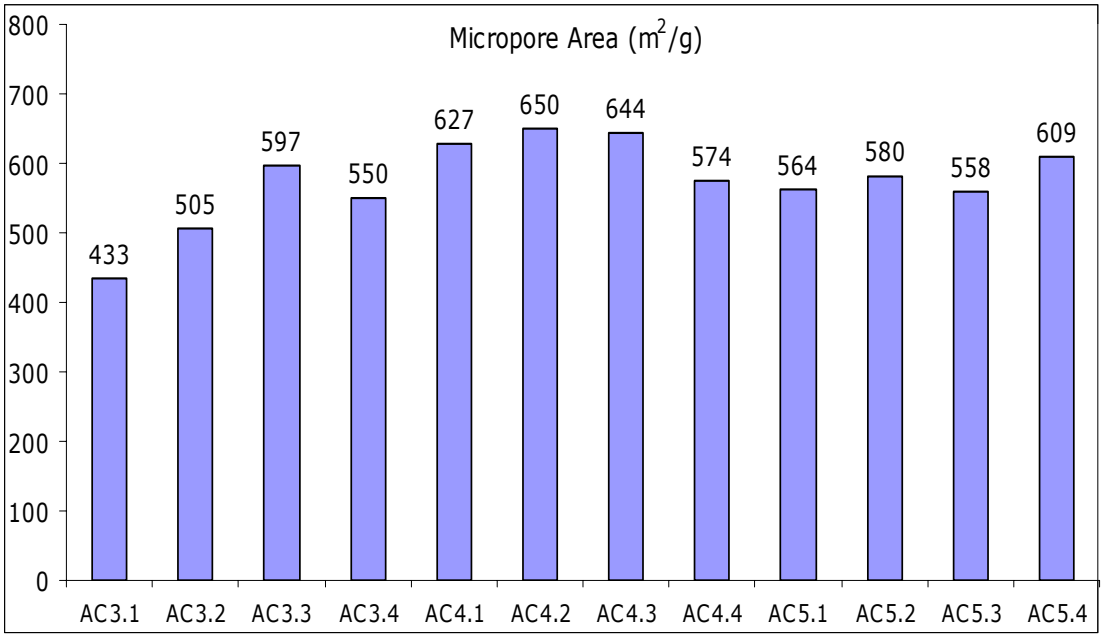

Figure 6.8 Micropore Area Values From CO_2 Adsorption at 0°C

Micropore area values of the samples are shown in the Figure 6.8. Similar to BET area, the highest micropore area, 650 m^2/g, was obtained from the AC4.2 sample and the lowest micropore area 433 m^2/g, was obtained from the AC3.1 sample. Also, similar to BET area, AC3 and AC4 series values gave a maximum. The difference from BET area, AC5 series do not give a minimum.

Micropore volume of the samples are shown in Figure 6.9. Micropre volume values are in the range of 0.16-0.32 cm^3/g. As it is shown from the figure micropore volume values graph is similar with micropore area.

BET equation has been used extensively to determine surface areas of activated carbons from nitrogen adsorption isotherms measured at -195.6°C. It is now generally agreed that N_2 adsorption at -195.6°C does not measure the total surface area of activated carbons for two important reasons. First, due to

the activated diffusion limitations, N_2 molecules at -195.6°C do not posses enough kinetic energy to readily penetrate into the micropores. Thus, impractically long periods are required for equilibrium to establish. Secondly, the micropores undergo some decrease in their size at low temperatures. On the other hand, in some cases, the CO_2 areas greatly exceed those determined from N_2 adsorption at -195.6°C for two reasons. First, minimum dimension of a CO_2 is smaller than that of N_2 molecule. Second, kinetic energy of CO_2 molecules at the adsorption temperatures used far exceeds that of N_2 molecules at -195.6°C. Consequently, rate of diffusion of CO_2 into the activated carbon micropores will be significantly higher than that of N_2.

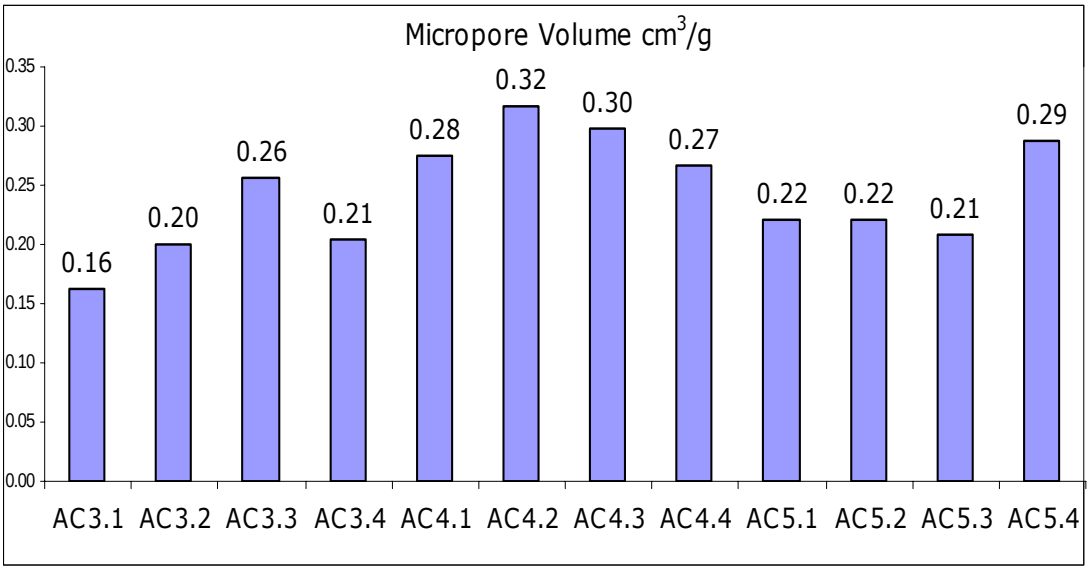

Figure 6.9 Micropore Volume Values From CO_2 Adsorption at 0°C

Other interpratation have also been found in literature that CO_2 adsorption may be influenced by the quadropole moment of CO_2 molecule interacting with the oxygen functionalities present on the carbon surface and

that higher surface area may be caused by a CO_2 induced swelling effect (Senel, 1994). CO_2 can measure pores down to 4-5 °A while BET can measure pores down to 10 °A.

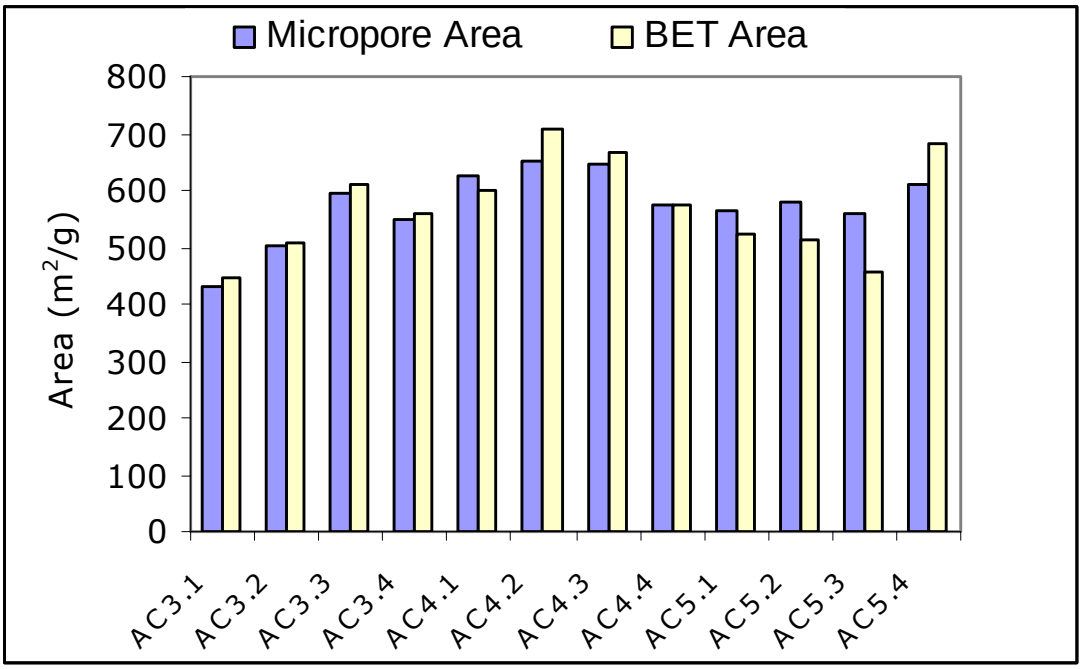

Figure 6.10 Comparison of BET and D-R Results

As it is shown in the Figure 6.10, for AC5.1, AC5.2 and AC5.3 samples micropore areas are greater than BET areas. Micropore area values do not increase significantly with the increasing carbonization time while BET are values decrease. Mesopore area values of the AC5 series are increasing with the increasing carbonization time.

The decrease of BET values for the samples AC5.1, AC5.2 and AC5.3 might be due to enlargement of the pores diameters down to 10A° for the

carbonization time up to 180 minutes. During this enlargement, the pores diameters smaller than 10A° can not be measured with N_2, so surface area of the smaller pores are not measurable. After 180 minutes for the sample AC5.4, there is 50 m^2/g increase in the micropore area value. For the same sample, increase in BET area value is about 220 m^2/g. The huge increase in BET can be explained as follows; the pores that are smaller than 10A° in diameter begin to enlarge after 180 minutes and this pores are detected by BET maesurement, so between 180 and 210 min. more pores smaller than 4-5 A° in diameter also enlarged so 50m^2/g more micropore surface is measured by CO_2.

6.2.3. Characterization of Activated Carbons by Mercury Intrusion Porosimetry

Macropore volume, macropore surface area and the apparent density values of the samples are given in Table 6.1. As it is seen in Table 6.1 macropore area and volume values of he samples are in the range of 0.2-1 m^2/g and 0.016-0.072 cm^3/g, respectively. It can be said that, there is no significant contribution of macropore surface area of the samples to the total surface area. However, macropore volumes of the samples are 5-20% of the total pore volume and these ratios have a significant contribution to the total pore volume of the samples.

Table 6.1 Mercury Porosimetry Results of Activated Carbons

Sample	S macro (m^2/g)	V macro (cm^3/g)	Apparent Density (g/cm^3)
AC3.1	0.65	0.030	1.1432
AC3.2	0.55	0.028	1.1286
AC3.3	0.97	0.063	0.9136
AC3.4	0.49	0.032	1.1797
AC4.1	0.58	0.062	0.9268
AC4.2	0.36	0.015	0.8531
AC4.3	0.45	0.026	0.7192
AC4.4	0.46	0.052	0.7432
AC5.1	0.68	0.038	1.3093
AC5.2	0.69	0.072	0.5978
AC5.3	0.50	0.045	1.2022
AC5.4	0.20	0.032	0.9934

6.2.4 Pore Volume Distribution of the Activated Carbons

The pore volume of the activated carbons determined as described above, in the macro, meso and micropore ranges are given in Table 6.2. In this table pore volume of all products and percentages corresponding to each pore range are given. As it is seen in the table, all the samples have at least 67% micropore volume of the total volume. As indicated in nitrogen adsorption isotherms, this values show that majority pores are in micropore region. Percentage of mesopore volume of the samples does not change significantly.

Table 6.2 Pore Volume Distributions of Activated Carbons

Sample	V macro (cm^3/g) *	V meso (cm^3/g) **	V micro (cm^3/g) ***	V total (cm^3/g)	**V macro (%)**	**V meso (%)**	**V micro (%)**
AC3.1	0.031	0.030	0.163	0.224	13.69	13.42	72.90
AC3.2	0.028	0.037	0.199	0.264	10.75	13.93	75.32
AC3.3	0.064	0.038	0.257	0.358	17.74	10.47	71.79
AC3.4	0.032	0.038	0.205	0.275	11.69	13.66	74.65
AC4.1	0.063	0.038	0.276	0.376	16.67	9.97	73.37
AC4.2	0.016	0.051	0.317	0.384	4.11	13.34	82.55
AC4.3	0.027	0.045	0.298	0.369	7.23	12.08	80.69
AC4.4	0.052	0.032	0.266	0.350	14.86	9.14	76.00
AC5.1	0.039	0.034	0.221	0.294	13.10	11.57	75.32
AC5.2	0.072	0.037	0.220	0.329	21.95	11.16	66.89
AC5.3	0.045	0.038	0.209	0.291	15.38	12.90	71.72
AC5.4	0.033	0.043	0.288	0.364	8.94	11.83	79.23

* Calculated from Mercury Intrusion Porosimetry

** Calculated from N_2 Ads./Des. at -195.6°C

*** Calculated from CO_2 Ads. at 0°C

6.2.5. Density and Total Pore Volume Determinations

True densities values of the activated carbons are determined at room temperature by Helium Pycnometry as explained in section 5.3.4 and are shown in Figure 6.11.

As it is shown in figure true density values of the samples are in the range of 1.5-1.8 g/cm^3 and increasing with the increasing carbonization

temperature. As carbonization temperature increases yield values decrease. Decrease of yield values means that pores are getting wider. As a result of enlargement of pore sizes the volume occupied by the carbon skeleton decreases. Using true and apparent densities of the products total open pore volume of the activated carbons were calculated as described in Section 4.4.

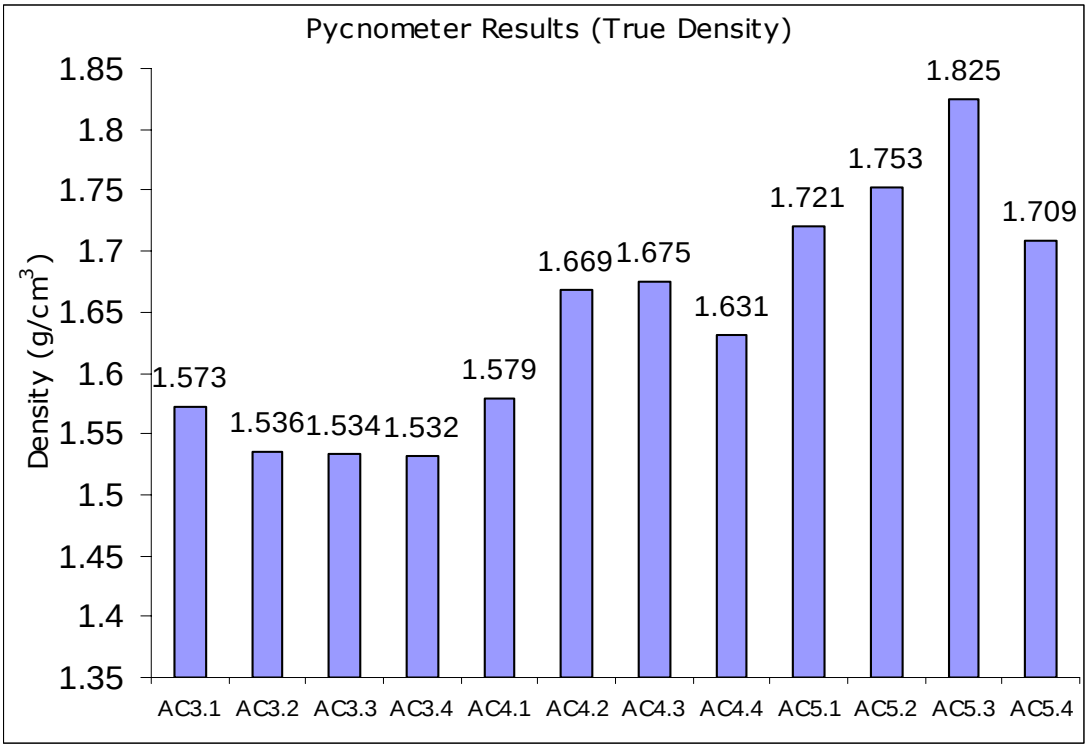

Figure 6.11 True Density Values of the Activated Carbons

In Table 6.3 total pore volume and porosity calculated as described in Section 4.4 are given.

Table 6.3 Densities and Total Pore Volumes of Products

Sample	Apparent Density (g/cm^3)	True Density (g/cm^3)	Porosity (%)	Total Pore Volume (cm^3/g)
AC3.1	1.1432	1.573	27.0	0.239
AC3.2	1.1286	1.536	26.5	0.235
AC3.3	0.9136	1.534	40.0	0.443
AC3.4	1.1797	1.532	23.0	0.195
AC4.1	0.9268	1.579	41.0	0.446
AC4.2	0.8531	1.669	49.0	0.573
AC4.3	0.7192	1.675	57.0	0.793
AC4.4	0.7432	1.631	54.0	0.732
AC5.1	1.3093	1.721	24.0	0.183
AC5.2	0.5978	1.753	66.0	1.102
AC5.3	1.2022	1.825	34.0	0.284
AC5.4	0.9934	1.709	42.0	0.422

The total pore volume evaluated in this method has shown some differences with that of obtained from the cumulative pore volumes (by adding macro, meso and micropore volumes).

This can be attributed to experimental errors, to the assumptions and to the physical constants involved in the methods. Table 6.4 shows the total pore volume calculated by using equation 4.16 and total pore volume calculated by adding macro, meso and micropore volumes.

Table 6.4 Comparison of Total Pore Volumes of the Samples

Sample Code	Total Pore Volume Calculated Using Eqn.4.16 (cm^3/g)	Total Pore Volume Calculated By Adding Volumes (cm^3/g)
AC3.1	0.239	0.224
AC3.2	0.235	0.264
AC3.3	0.443	0.358
AC3.4	0.195	0.275
AC4.1	0.446	0.376
AC4.2	0.573	0.384
AC4.3	0.793	0.369
AC4.4	0.732	0.350
AC5.1	0.183	0.294
AC5.2	1.102	0.329
AC5.3	0.284	0.291
AC5.4	0.422	0.364

6.3. TGA of Raw and Impregnated Apricot Stones

TGA experiments were carried out to obtain the yield values for each carbonization time and carbonization temperature. It was difficult to obtain the yield values from the experiments which are done with the experimental set-up.

TGA experiments were done at same experimental conditions with respect to carbonization time and temperature, particle size, N_2 flow rate, impregnation ratio and heating rate. Yield values of samples, for acid impregnated and raw apricot stones, for different temperature and time are given in Table 6.5, Table 6.6 and Table 6.7.

Table 6.5 Yield Values (%) of Samples for T=300°C

	AC 3.1	AC 3.2	AC 3.3	AC 3.4
Acid Impregnated	55	54.7	54.1	54
Raw Apricot Stones	48.48	46.5	45.13	44.81

Table 6.6 Yield Values (%) of Samples for T=400°C

	AC 4.1	AC 4.2	AC 4.3	AC 4.4
Acid Impregnated	49.6	49.3	49	48.9
Raw Apricot Stones	32.93	32,09	30.70	30.16

Table 6.7 Yield Values (%) of Samples for T=500°C

	AC 5.1	AC 5.2	AC 5.3	AC 5.4
Acid Impregnated	46,3	46	45.6	45.5
Raw Apricot Stones	28.95	28.6	28.22	28.08

As it is seen from the tables, yield values of phosphoric acid impregnated samples are higher than that of raw apricot stones for the same temperature. Yield values are decreasing with the increasing carbonization temperature and decreasing slightly with the increasing carbonization time for both acid impregnated and raw apricot stones samples.

After adding phosphoric acid the depolymerization reactions (as indicated in Section 2.1 and 3.2.2.1) inside the apricot stones during the carbonization under temperature are affected. Phosphoric acid (H_3PO_4) restricts the formation of tar (Section 3.2.2.1) and volatile materials do not evacuate from the structure. Therefore, yield values of acid impregnated samples increase with respect to raw samples.

TGA figures of the acid impregnated and raw apricot stones are given in Appendix F.

CHAPTER VII

CONCLUSIONS

From the results of this work, it is concluded that apricot stones can be used as raw material for the production of activated carbon. N_2 and CO_2 isotherms, together with the mercury porosimetry measurements show that activated carbons obtained from apricot stones, by chemical activation technique, have a certain degree of porosity, located mainly in micro size of pores.

One of the novelties of this work is the use of phosphoric acid (H_3PO_4) as the activating agent during carbonization. Results showed that, pretreatment of the apricot stones with H_3PO_4 solution before carbonization increased the values of surface area of the activated carbon produced at relatively low temperatures. The products obtained from H_3PO_4 impregnated apricot stones gave surface area values over 700m^2/g at carbonization temperature of 400^oC.

Phosphoric acid impregnation improved the micropore structure and over 90 percent of the surface areas of the products were found to correspond to

pores having diameters less than 2 nm. The remaining 10 percent of the surface areas of the products were found to correspond to pores having diameters between 2 and 50 nm.

From the chemical analysis of the products it is concluded that, ash contents are slightly high with respect to typical values. The lowest ash content value obtained as 3.2 percent and the highest value obtained as 7.7 percent. These results can be attributed to phosphoric acid (H_3PO_4), high heating rate and high impregnation ratio. Yield values from TGA experiments showed that phosphoric acid (H_3PO_4) increases the yield values of apricot stones. So it can be concluded that phosphoric acid (H_3PO_4) restricts the formation of tar during the carbonization.

CO_2 adsorption results showed that micropore area values for the products, except AC 3.1 sample, are close to each other for the same carbonization temperature. It is indicate that microporosity develop at low carbonization temperature and carbonization time.

CHAPTER VIII

RECOMMENDATIONS

Activated carbon has several industrial applications depending on its porous structure and adsorption capacity. To increase the BET surface area value of the activated carbon produced from apricot stones, it is recommended to carry out experiments with different experimental parameters. Some of the most critical parameters are the impregnation ratio, heating rate, carbonization temperature and carbonization time.

The future efforts in this field should include the investigation of the effect of phosphoric acid. To get more idea about the kinetics of carbonization of impregnated sample, it is better to analyze the gaseous products. Therefore, it is also recommended to carry out the carbonization experiments in fixed bed reactor.

To decrease the ash content value, it is recommended to change the heating rate and apricot stones / phosphoric acid impregnation ratio.

REFERENCES

1. Agrawal, R.K. and Mc Cluskey, R.J., "The Low Pressure Pyrolysis of Newsprint", *J. of AppI. Polv. Sci*., Vol. 27, pp.367-382. (1983)

2. Agrawal, R.K., "Kinetics of Reactions Involved in Pyrolysis of Cellulose I. The Three Reaction Model", *Can. J. of Chem. Eng.,* Vol. 66, pp.403-412. (1988a)

3. Agrawal, R.K., "Kinetics of Reactions Involved in Pyrolysis of Cellulose II. The Modified Kilzer-Broido Model", *Can. J. of Chem. Eng.,* Vol. 66, pp.413-418. (1988b)

4. Asma, B.M., Apricot Production. Evin Ofset, Malatya, Turkey (2000).

5. Baçaoui, A., Yaacoubi, A., Dahbi, A., Bennouna, C., Phan Tan Luu, R., Maldonado- Hodar, F.J., Rivera-Utrilla, J. and Moreno-Castilla, C., ”Optimization of Conditions for the Preparation of Activated Carbons from Olive-Waste Cakes”, *Carbon* Vol. 39, pp.425-432. (2001)

6. Balcı, S., PhD Dissertation, METU, Ankara (1992)

7. Balcı, S., Doğu, T. And Yücel, H., “Characterization of Activated Carbon Produced from Almond Shelland Hazelnut Shell”, *J. Chem. Tech. Biotechnol.* Vol.60, pp.419-426. (1994)

8. Barrett, E. P., Joyner, L. G. and Halenda, P. P., “The Determination of Pore Volume and Area Distribution in Porous Substances. I. Computations from Nitrogen Isotherms”, *J. Am. Chem. Soc.*, Vol. 73, pp.373-380. (1951)

9. Basso, M. C., Cerrella, E. G. and Cukierman, A. L., “Activated Carbons from a Rapidly Renewable Biosource for Removal of Cadmium(II) and Nickel(II) Ions from Dilute Aqueous Solutions”, *Ind. Eng. Chem. Res.* Vol. 41, pp.180-189. (2002)

10. Benaddi, H., Bandosz, T. J., Jagiello, J., Schwarz, J. A., Rouzaud, J. N., Legras, D. and Béguin, F., “Surface Functionality and Porosity of Activated Carbons Obtained from Chemical Activation of Wood”, *Carbon* Vol. 38, pp.669-674. (2000)

11. Bevla, F. R., Rico, D. P. and Gomis, A. F. M., “ Activated Carbon from Almond Shells. Chemical Activation. 1. Activating Reagent Selection and

Variables Influence", *Ind. Eng. Chem. Prod. Res. Dev.* Vol. 23, pp.266-269. (1984)

12. Bevla, F. R., Rico, D. P. and Gomis, A. F. M., " Activated Carbon from Almond Shells. Chemical Activation. 2. $ZnCl_2$ Activation Temperature Influence", *Ind. Eng. Chem. Prod. Res. Dev.* Vol. 23, pp.269-271. (1984)

13. Blasco, J. M., Cordero, T., Gomez Martin, J. P. and Rodriguez, J. J., "A Kinetic on Chemical Activation of Holm Oak Wood", *J. of Anal. and Appl. Pyroly.*, Vol. 18, pp.117-126. (1990)

14. Broekhoff, J. C. P. and Linsen, B. G., Physical and Chemical Aspects of Adsorbents and Catalysts, ed. B. G. Linsen, Academic Press, New York. (1970)

15. Browning, B. L., The Chemistry of Wood., Interscience Pub., New York, London. (1963)

16. Brunauer, S., Demming, L. S., Demming, W. S. and Teller, E., *J. Am. Chem. Soc.*, Vol. 62, pp.1723. (1940)

17. Cookson, J. T., Carbon Adsorption Handbook. (Edited by Cheremisinoff, P. N. and Ellerbusch, F.) pp.241-279, Ann Arbor Sci., Michigan. (1980)

18. Cranston, R. W. And Inkley, F. A., *Adv. Catal.* Vol. 9, pp.143. (1957)

19. Dubinin, M. M. And Radushkevich, L. V., *Proc. Acad. Sci., SSSR*., Vol.55, pp.331. (1947)

20. Dubinin, M. M. and Astakhov, V. A., *Inz. Nauk., SSSR.*, Vol. 55, pp.5. (1971)

21. Dubinin, M. M., "On Methods for Estimating Micropore Parameters of Carbon Adsorbents", *Carbon*, Vol. 26, pp.97-110. (1988)

22. Faust, S. D. and Aly, O. M., Chemistry of Water Treatment, Butter Wort Pub., Woburn. (1983)

23. Franklin, R. E., "Crystallite Growth in Graphitizing and Nongraphitizing Carbons", *Proc. Roy. Soc.* (London) A 209, 196-218. (1951)

24. Girgis, B. S. and Daifullah, A. A., "Removal of Some Substituted Phenols by Activated Carbon Obtained from Agricultural Waste", *Wat. Res.* Vol. 32, pp.1169-1177, (1998)

25. Gregg, S. J. and Sign, K.S.W., Adsorption, Surface and Porosity, New York Academic Press. (1967)

26. Gregg, S. J. and Sign, K.S.W., Adsorption, Surface and Porosity, 2nd. Edn, New York Academic Press. (1982)

27. Halsey, G. D., *J. Chem. Phys.*, Vol. 16, pp.931. (1948)

28. Hassler, J. W., Purification with Activated Carbon, Chem. Pub. Co., New York. (1974)

29. Holden, M. J., "Manufacture and Uses of Activated Carbon", *Eff. and Water Treat. J.* Vol. 22, pp.27-31. (1982)

30. Zhonghua Hu, Srinivasan, M. P. and Yaming Ni, "Novel Activation Process for Preparing Highly Microporous and Mesoporous Activated Carbons", *Carbon* Vol. 39, pp.877-886. (2001)

31. Iniesta, E., Sanchez, F., Garcia, A. N. and Marcilla, A., "Yields and CO_2 Reactivity of Chars from Almond Shells Obtained by a Two Heating Step Carbonization Process. Effect of Different Chemical Pre-Treatments and Ash Content", *J.of Anal. and Applied Pyrolysis* Vol. 58-59, pp.983-994. (2001)

32. Laine, J., Calafat, A. and Labady, M., "Preparation and Characterization of Activated Carbons from Coconut Shell Impregnated with Phosphoric Acid", *Carbon* Vol. 27, No.2 pp.191-195. (1989)

33. Livingstone, H. K., *J. Colloid. Sci.*, Vol.4, pp.1447. (1949)

34. Lumadede, M. H., MSc. Dissertation, METU, Ankara (2002)

35. Martin, A. E., Chemistry of Coal Utilization, 2nd Supp. Vol., John Wiley and Sons Inc. (1981)

36. Orr, C. and Dalla, V. J. M., Fine Particle Measurement, Mc Millian, New York. (1959)

37. Özer, A., Çam, G., "The Determination of Surface Area and Color Adsorption Capacity of Activated Carbon from Sugar Beet Pulp Treated with Phosphoric Acid", *F. Ü. Müh. Bil. Der.* Vol.14(1), pp.191-197. (2002)

38. Polanyi, M., *Trans. Faraday Soc.,* Vol.28, pp.316. (1932)

39. Pierce, C., Smith, R. N., *J. Phys. Chem*., Vol. 57, pp.56. (1953)

40. Reinoso, R. F., Martinez, M. J. M., Sabio, M. M., "A Comparison of the Porous Texture of Two CO_2 Activated Botanic Materials", *Carbon,* Vol. 23 pp.19-24. (1985)

41. Ritter, H. L., Drake, L. E., "Macropore Size distribution in Some Typical Porous Substances", *Ind. Eng. Chem. Anal. Ed.*, Vol. 17, pp.782. (1945)

42. Rodriguez Reinoso, F., "An Overview of Methods for the Characterization of Activated Carbons", *Pure and Appl. Chem.* Vol. 61, No.11, pp.1859-1866. (1989)

43. Roberts, A. F., "A Review of A Kinetic Data for the Pyrolysis of Wood and Related Substances", *Comb. And Flame,* Vol. 14, pp.261-272. (1970)

44. Ruthven, D. M., Principle of Adsorption and Adsorption Process, John Wiley and Sons, New York, (1984)

45. Sánchez,A. R., Elguézabal, A. A. and Saenz, L. L. T., "CO_2 Activation of Char from *Quercus Agrifolia* Wood Waste", *Carbon,* Vol. 39, pp.1367-1377. (2001)

46. Schewenker, Jr. R. P. and Pascu, E., "Pyrolytic Degradation Products of Cellulose", *Chem. Eng. Data Ser.2,* No.1, pp.83-88. (1957)

47 Şenel, G. İ., PhD Dissertation, METU, Ankara (1994)

48. Selles Perez, M. and Martin Martinez, M. "Application of α and n Plots to N_2 Adsorption Isotherms of Activated Carbon", *J. Chem. Soc. Faraday Trans.* Vol. 87, No.8, pp.1237-1243. (1991)

49. Smisek, M. And Cerny, S., Active Carbon Manufacture, Properties and Aplications, Elsevier Pub., Comp., New York. (1970)

50. Solano, L. A., Gonzalez, L. J. de D., Sabio, M. M., "Active Carbons from Almond Shells as Adsorbents in Gas and Liquid Phases", *J. Chem. Tech. Biotech*. Vol. 30, pp.65-72. (1980)

51. Toles, C. A., Marshall, W. E. and Johns, M. M., "Granular Activated Carbons from Nutshells for the Uptake of Metals and Organic Compounds", *Carbon*, Vol.35, No.9, pp.1407-1414. (1997)

52. Toles, C. A., Marshall, W. E., Johns, M. M., Wartelle, L. H. and McAloon A., "Acid-Activated Carbons from Almond Shells: Physical, Chemical and Adsorptive Properties and Estimated Cost of Production", *Bioresource Technology*, Vol. 71, Issue 1, pp.87-92. (2000)

53. TS 6879, Turkish Standards Institution (TSE). Activated Carbon Determination of Total Ash Content

54. TS 5896, Turkish Standards Institution (TSE). Activated Carbon Determination of pH value.

55. Yang, T. and Lua, A. C., "Characteristics of Activated Carbons Prepared from Pistachio-Nut Shells by Physical Activation", *Journal of Colloid and Interface Science,* Vol. 267, Issue 2, pp.408-417. (2003)

56. Walker, P. L. and Shelef, M., *Chemistry and Physics of Carbon,* Vol.4, pp. 287-383

57. Washburn, E. W., "Note on A Method of Determining the Distribution of Pore Sizes in a Porous Material", *Proc. Nat. Acad. Sci.*, Vol. 7, pp.115-116. (1921)

58. Wigmans, T., Carbon and Coal Gasification. (Edited by Figueriedo, J. L. and Moulijn, J. A.,), pp.559-601, Martinus Nijhoff Pub., Lancaster. (1985)

59. Wolff, W. F., "A Model of Active Carbon", *J. Phys. Chem.* Vol. 63, pp.653-659. (1959)

APPENDIX A

ANALYSIS OF MERCURY POROSIMETRY DATA

A.1. Analysis of Macropores

In the present study, analysis of macropore volume and areas were determined by using a commercial mercury porosimeter which involves the technique of forcing mercury under increasing pressure into successively smaller pores of the sample.

If a pore or void space is considered to be circular in cross section, the surface tension γ of the mercury acts along the circle of contact for a length equal to perimeter of the circle. If r_p is the pore radius, the force tending to squeeze the liquid out of the pore normal to the plane of the circle of contact may be written $-2\pi r_p \gamma \cos\theta$, where θ is contact angle (Ritter and Drake, 1945). The negative sign enters because for θ greater than 90°, the term $2\pi r_p \gamma \cos\theta$, is intrinsically positive. The opposing force, the force due to an externally applied pressure, acts over the area of the circle of contact and

is $\Pi r^2_p P$ where P is the applied pressure. At equilibrium the opposing forces are equal; thus

$$-2\pi r_p \gamma \cos\theta = \Pi r_p P \qquad (A.1)$$

or, replacing $Dp=2r_p$, Washburn equation can be obtained (Washburn, 1921).

$$Dp = \frac{-4\gamma Cos\theta}{P} \qquad (A.2)$$

Taking the γ and θ values as 485 dynes/cm and 130° (Orr, 1959) respectively, and substituting info the equation A.1,

$$Dp(\mu m) = \frac{-4x485\left(\frac{dynes}{cm}\right)x10^{4}\left(\frac{\mu m}{cm}\right)x-0.6428}{P(psia)x6.8948\ x10^{4}\left(\frac{dynes}{cm.psia}\right)} \qquad (A.3)$$

which, in simplified form, can be given as;

$$Dp = \frac{180(\mu m.psia)}{P(psia)} \qquad (A.4)$$

Pore surface area can be calculated from the PV work expanded in forcing mercury into the pores. The work dW required to immerse an area dA of pore wall is expressed by

$$dW = \gamma \cos\theta\, dS = -P\, dV \qquad (A.5)$$

the total cumulative area up to Vmax then

$$S = \frac{1}{\gamma Cos \quad \theta} \int_{0}^{V \max} PdV \qquad (A.6)$$

Taking the surface tension and contact angle values given above, surface area per unit weight of material,

$$S = \frac{0.0225}{m} \int_{V \min}^{V \max} PdV \qquad (A.7)$$

In the present study, Mercury intrusion pressures of 3600 psia and 22 psia which correspond to pores diameters of 0.05 and 8.18 μm. according to equation A.4 were taken as the upper and the lower limits for the determination of the macropores. Then, cumulatively obtained volume and area values were used to estimate the macropore volume and areas.

$$Vmacro = \left[Vcum \Big|_{\substack{P=3600 \ psi \\ dp=0.05 \ \mu m}} - Vcum \Big|_{\substack{P=22 \ psi \\ dp=8.18 \ \mu m}} \right] (cm^3 / g)$$

A.8)

$$Smacro = \left[Scum \Big|_{\substack{P=3600 \ psi \\ dp=0.05 \ \mu m}} - Scum \Big|_{\substack{P=22 \ psi \\ dp=8.18 \ \mu m}} \right] (m^2 / g) \qquad (A.9)$$

A.2. Determination of Apparent Density

In this study, apparent density of all the samples was calculated from the mercury intrusion measurements at 22 psia. Since, it was determined that at that particular pressure, interparticle space of the particles (0.50-0.25 µm in diameter) was completely filled with mercury. In the determination of

apparent density the following procedure was used:

1- Weight of sample= W_s

2- Weight of sealed, empty penetrometer = W_p

3- Weight of penetrometer and sample = W_s+W_p

4- Weight of penetrometer, sample and mercury: = $W_s+W_p+W_{Hg}$

5- Weight of mercury (4-3): $=W_{Hg}= (W_s+W_p+W_{Hg})-(W_s+W_p)$

6- Volume of mercury (5/ density of mercury):

$$V_{Hg} =W_{Hg} / \rho_{Hg} \qquad (A.10)$$

7 - Volume of Penetrometer = V_p

Volume of penetrometer was obtained from the calibration runs, by measuring the mercury displaced in empty penetrometer.

8- Volume of sample (7-6)= $V_s= V_p- V_{Hg}$

9- Pore volume, mercury displaced in penetrometer stern at 22 psi = V_p

10- Apparent density of the sample at 22 psi:

$$\rho_{Hg} =W_s / (V_s-V_p) \qquad (A.11)$$

A.3. Sample Calculation

Sample Code: AC 5.1 (Carbonization Temperature=500°C, Carbonization Time=90 min)

A.3.1. Calculation of Macropore Volume and Area

Cumulative Volume Intruded up to 3600 psia (down to D_p=0.05μm)=0.19 cm^3/g

Cumulative Volume Intruded up to 22 psia (down to D_p=8.18μm)=0.1515 cm^3/g

Replacing these quantities into equation A.8: V_{macro}= 0.19-0.1515=0.0385 cm^3/g

Cumulative Pore Surface Area up to 3600 psia(down to D_p=0.05μm)=0.7m^2/g

Cumulative Pore Surface Area up to 22 psia(down to D_p=8.18μm)=0.0148m^2/g

Replacing these quantities into equation A.9: S_{macro}= 0.7-0.0148 = 0.685 m^2/g

A.3.2. Calculation of Apparent Density

1- W_s= 0.2005 g

2- W_p= 67.8877 g

3- W_s+W_p= 68.0882 g

4- $W_s+W_p+W_{Hg}$= 117.9253 g

5- W_{Hg}=($W_s+W_p+W_{Hg}$)-(W_s+W_p)= 49.8371 g

Density of Mercury = 13.5487 g/ cm^3 (at 19°C)

6- V_{Hg}= 3.6784 cm^3

7- V_p= 3.8315 cm^3

8- V_s= 0.1531 cm^3

9- Pore volume, mercury displaced in penetrometer stem at 22 psi:

V_p= 0.2634 cm^3/g x 0.2005=0.0528 cm^3

10- Apparent density of the sample at 22 psi:

=0.2005/ (0.1531-0.0528) = 1.999 g/ cm^3

APPENDIX B

ANALYSIS OF N_2 SORPTION DATA

B.1. Analysis of Mesopores

Adsorption studies reading to measurements of pore sizes and pore size distributions generally make use of the Kelvin equation B.1 which relates the equilibrium vapor pressure of a curved surface such as that of a liquid in a capillary or pore, to the equilibrium pressure of the same liquid on a plane surface (Gregg and Sing, 1982).

$$\ln \frac{P}{Po} = \frac{-2\gamma VmolCos\,\theta}{r_p RT} \qquad \text{(B.1)}$$

where P is the equilibrium vapor pressure of the liquid contained in a narrow pore of radius r_p and Po is the equilibrium pressure of the same liquid at a plane surface. The terms γ and V_{mol} are surface tension and molar volume of the liquid, respectively. θ is the contact (wetting) angle with which the liquid meets the pore wall.

If the transfer of d_n moles of vapor in equilibrium with the bulk liquid at pressure Po into a pore where the equilibrium pressure P is considered, this process consists of three steps: evaporation from the bulk liquid, expansion of the vapor from Po to P and condensation into the pore. The first and third of these steps are equilibrium processes and are therefore accompanied by a zero free energy change, whereas the free energy change for the second step is described by

$$dG = \left(RT \ \ln\left(\frac{P}{Po} \right) \right) dn \tag{B.2}$$

When the adsorbate condenses in the pore

$$dG = -\left(\gamma Cos \ \theta \right) dS \tag{B.3}$$

where dS is the change in the film-vapor interfacial area and θ is the wetting angle which is taken to be zero since the liquid is assumed to wet completely the adsorbed film. Equations B.2 and B.3, when combined

$$\frac{dn}{dS} = \frac{-\gamma}{RT \ \ln\left(P / Po \right)} \tag{B.4}$$

The volume of liquid adsorbate which condenses in a pore of volume V_p is given by

$$dVp = Vmoldn \tag{B.5}$$

Substituting equation B.4 into B.5 gives

$$\frac{dVp}{dS} = \frac{-\gamma \ Vmol}{RT \ \ln\left(P / Po \right)} \tag{B.6}$$

The ratio of volume to area within a pore depends upon the geometry. When the shapes of the pores are highly irregular or consisting of a mixture of regular geometries, the volume to area ratio can be too complex to express mathematically. In these cases, or in the absence of specific knowledge of the pore geometry, the assumption of cylindrical pores is usually made. Since the ratio of volume to area for cylinders is r/2, the equation B.6 gives the Kelvin equation;

$$\ln\left(\frac{P}{Po}\right) = \frac{-2\gamma Vmol}{rRT} \tag{B.7}$$

For nitrogen as the adsorbate at its normal boiling point of -195.6°C, the Kelvin equation can be written as

$$r_k = \frac{2\left(8.85\ \frac{erg}{cm^2}\right)\left(34.6\ \frac{cm^3}{mol}\right)\left(\frac{10^8\ {}^oA}{cm}\right)}{\left(8.314\ x10^7\ \frac{erg}{Kmol}\right)(77\ K)(2.303)\log\left(P_o\ /\ P\right)} \tag{B.8}$$

where 8.85 erg/cm^2 is the surface tension and 34.6 cm^3 is the molar volume of liquid nitrogen at -195.6°C. Then equation B.9 can be found as

$$r_k = \frac{4.15}{\log(P_o\ /\ P)} \tag{B.9}$$

The term r_k indicates the radius into which condensation occurs at the required relative pressure. This radius, called the Kelvin radius or the critical radius, is not the actual pore radius since some adsorption has already occurred on the pore wall prior to condensation, leaving a center core or radius r_k. Alternatively, during desorption, an adsorbed film remains on the pore wall

when evaporation of the center core takes place. If the depth of the film when condensation or evaporation occurs is t, then the actual pore radius r_p is given by

$$r_p = r_k + t \qquad \text{(B.10)}$$

This equation can be used to calculate r_p but some means of evaluating t is required if the pore radius is to be determined. Using the assumption that the adsorbed film depth in a pore is the same as that on a plane surface for any value of relative pressure, one can write

$$t = \left(\frac{W_a}{W_m}\right)\tau \qquad \text{(B.11)}$$

Where W_a and W_m are, respectively, the quantity adsorbed at a particular relative pressure and the weight corresponding to the BET monolayer. Essentially equation B.11 asserts that the thickness of the adsorbed film is simply the number of layers times the thickness τ of one layer regardless of whether the film is in a pore or on a plane surface. The t value of τ can be calculated by considering the area S and volume V_{mol} occupied by one mole of liquid nitrogen if it were spread over a surface to the depth of one molecular layer

$$\tau = \frac{V_{mol}}{S} = \frac{(34.6\,x10^{24})A^3}{\left(16.2\,\frac{A^2}{mol}\right)\left(6.02\,x10^{23}\,\frac{1}{mol}\right)} = 3.54\,A \qquad \text{(B.12)}$$

On nonporous surfaces it has been shown that when the quantity W_a/W_m is plotted versus P/P_o the data all approximately fit a common type II curve above a relative pressure of 0.3 (Cranston and Inkley, 1957). The common curve is described closely by Halsey, (1948) equation which for nitrogen can be

written as

$$t = 3.54\left(\frac{5}{2.303\log\left(P_o / P\right)}\right)^{1/3} \tag{B.13}$$

The thickness of the adsorbed layer which is calculated for a particular relative pressure from the above equation which becomes thicker and thicker with successive increase in pressure, so that the measured quantity of gas adsorbed in a step is composed of a quantity equivalent to the liquid cores formed in that step plus the quantity adsorbed by the pore walls of pores whose cores have been formed in that and previous steps. Barrett Joyner and Halenda developed the method (BJH) which incorporates these ideas. The algorithm used on the ASAP 2000; the N_2 adsorption apparatus used in the present work, is an implementation of the BJH method. According to this method, ΔV_{gas}, the incremental volume: the change in adsorbed volume between two successive P/P_o values can be determined by subtracting the successive values. The ΔV_{gas} then, can be converted to ΔV_{liq} by multiplying by the liquid molar volume for nitrogen at standard temperature and pressure. This is given by

$$\Delta V_{liq} = \frac{\Delta V_{gas}\left(cm^3 / g\right)}{22414\left(cm^3 / mol - STP\right)}\left(34.6\left(cm^3 / mol\right)\right) = \Delta V_{gas}\left(1.54x10^{-3}\right) \tag{B.14}$$

The actual pore volume was evaluated by

$$\Delta V_{liq} = \pi r^2{}_{KAVE} + \Delta t \sum S \tag{B.15}$$

In this equation r_{KAVE} is the average Kelvin radius and the term $\Delta t\ \Sigma S$ is the product of the film area and the increase in the film depth, and since,

$$V_p = \pi r^2_{PAVE} L \quad \text{(B.16)}$$

where L is the pore length, by combining the equations, B.15 and B.16

$$V_p = \left(\frac{r_{PAVE}}{r_{KAVE}}\right)^2 \left[\Delta V_{liq} - \left(\Delta t \sum S\right)\left(10^{-4}\right)\right] \text{ (cm}^3\text{)} \quad \text{(B.17)}$$

The surface area of the pore walls can be calculated from the pore volume by

$$S = \frac{2V_p}{r_{PAVE}}\left(10^4\right) \text{ (m}^2\text{)} \quad \text{(B.18)}$$

Then, mesopore volume and surface areas were calculated by using the incremental pore volume and surface area values evaluated from the equations B.17 and B.18:

$$V_{meso} = \left[\sum V_p \Big|_{d_p = 0.002\mu m} - \sum V_p \Big|_{d_p = 0.05\mu m}\right] \text{(cm}^3\text{/g)} \quad \text{(B.19)}$$

$$S_{meso} = \left[\sum S \Big|_{d_p = 0.002\mu m} - \sum S \Big|_{d_p = 0.05\mu m}\right] \text{(m}^2\text{/g)} \quad \text{(B.20)}$$

B.2. Determination of BET Surface Area

BET surface areas of the samples can be obtained from the plot of $P/V(P_o-P)$ versus P/P_o plot, in the relative pressure range 0-0.2, using the following relation (Brunauer et al., 1938).

$$\frac{P}{V[P_O - P]} = \frac{1}{VmC} + \frac{C-1}{V_m C}\frac{P}{P_O} \quad \text{(B.21)}$$

The slope and intercept of this plot which are given as

$$S=\frac{C-1}{V_m C} \quad \text{and} \quad I=\frac{1}{VmC} \qquad \text{(B.22)}$$

an be used to evaluate BET surface area by the equation

$$S_{BET}=\frac{\left[\left(CSA_{N_2}\,nm^2\right)\left(6.023x10^{23}\left(1/mol\right)\right)\right]}{\left[\left(22414\left(cm^3/mol-STP\right)\right)\left(10^{18}\left(nm^2/m^2\right)\right)\left(\left(S+I\right)\left(g/cm^3-STP\right)\right)\right]} \qquad \text{(B.23)}$$

where CSA_{N2} is the cross sectional area of a nitrogen molecule.

B.3. Sample Calculation

Sample Code AC 3.2 (Carbonization Temperature=300°C, Carbonization Time=120 min.)

B.3.1. Calculation of Mesopore Volume and Area

Cumulative Mesopore Volume up to d_p=20 °A (2 nm)=0.03685 cm^3/g

Cumulative Mesopore Volume up to d_p=500 °A (50 nm)=0.00005 cm^3/g

Replacing these quantities into equation B.19:

V_{meso}= 0,03685-0,00005=0,0368 cm^3/g

Cumulative Pore Surface Area up to d_p=20 °A (2 nm)= 60.02m^2/g

Cumulative Pore Surface Area up to d_p=500 °A (50 nm)= 0.02m^2/g

Replacing these quantities into equation B.20:

S_{meso}= 62.02-0.02= 60 m^2/g

B.3.2. Calculation of BET Surface Area

S=Slope= 0.008638

I=Intercept= -0.000117

CSA_{N_2} =0.162 nm^2 (Walker et al., 1968)

Replacing these quantities into equation B.23:

S_{BET}= 510.86 m^2/g

APPENDIX C

ANALYSIS OF CO_2 ADSORPTION DATA

C.1. Analysis of Micropores

The micropore volume of the samples calculated by applying the Dubinin Radushkevich (D-R) equation to the CO_2 adsorption data in the relative pressure range $1x10^{-4}$ – $1x10^{-2}$

$$\log V = \log V_o - 2.303K\left(\frac{RT}{\beta}\right)^2\left[\log\frac{P_o}{P}\right]^2 (cm^3/gSTP) \qquad \text{(C.1)}$$

A plot of log V versus log $(P/P_o)^2$ gives straight line with an intercept of log V_o from which V_o, the micropore volume (cm^3/g STP) could be calculated. In this equation, β is a constant which is the ratio of the adsorption potentials. K is also a constant determined by the shape of the pore distribution curve. The micropore volume in the unit of (cm^3/g STP) which refers to the adsorbate state based on the ideal gas behavior at STP was also converted into the unit of (cm^3/g) which is based on the specific volume of the adsorbate in the adsorbed

state at 0°C by the following equation

$$V_o(cc/g) = \frac{V_o(cm^3/g - STP)MW_{CO_2}(g/mol)}{(22414\ (cm^3/mol - STP))(\rho_{CO_2}(g/cm^3))} \quad \text{(C.2)}$$

where ρ is the density of the CO_2 molecule. Micropore surface area or so called D-R surface area was then evaluated by

$$S_{DR} = \frac{(\sigma nm^2)V_o(cm^3/g - STP)(6.02\ x10^{23})}{(22414\ cm^3)(10^{18}\ nm^2/m^2)} \quad \text{(C.3)}$$

where σ is the cross sectional area of a CO_2 molecule.

C.2. Sample Calculation

Sample Code: AC 3.4

Micropore volume (cm^3/g STP) directly obtained from the ASAP 2000M; Micropore Analysis unit which processed the collected CO_2 adsorption data. In these calculations;

Saturation pressure of CO_2 =26142.000 mm Hg at 0°C (Micromeritics ASAP 2000, User Manual, Appendix C, 1993)

Absolute Pressure Range= 28.69383- 352.1831 mm Hg

Corresponding Relative Pressure Range= $5.9x10^{-4}$- $7.3x10^{-3}$

V_{micro}= 120.4527 cm^3/g STP

Corresponding micropore volume in the units of cm^3/g was evaluated by taking

Density of CO_2 at 0^oC=1.181 g/cm^3 (Micromeritics ASAP 2000, User Manual, Appendix C, 1993) and replacing into equation C.2:

V_{micro}= 0.205 cm^3/g

Micropore surface area (D-R surface area) obtained by taking

Cross Sectional Area of CO_2 molecule =0.17 nm^2 (Micromeritics ASAP 2000, User Manual, Appendix C, 1993)

Replacing into equation C.3

S_{D-R}= 550 m^2/g

APPENDIX D

ANALYSIS OF HELIUM PYCNOMETER DATA

D.1 Determination of True Density

True densities of the samples were determined by helium displacement method. A commercial He Pycnometer apparatus "The Multivolume Pycnometer 1305" manufactured by Micromeritics Co., USA was used to measure true densities of the activated carbons.

Assume that both V_{CELL} and V_{EXP} are at ambient pressure P_a, are at ambient temperature T_a, and that the valve is then closed. V_{CELL} is then charged to an elevated pressure P_1. The mass balance equation across the sample cell, V_{CELL} is

$$P_1\left(V_{CELL} - V_{SAMP}\right) = n_C R T_a \tag{D.1}$$

where

n_C= the number of moles of gas in the sample cell,

R= the gas constant, and

T_a= the ambient temperature

The mass equation for the expansion volume is

$$P_a V_{EXP} = n_E RT_a \tag{D.2}$$

where

n_E= the number of moles of gas in the expansion volume.

When the valve is opened, the pressure will fall to an intermediate value, P_2, and the mass balance equation becomes

$$P_2\left(V_{CELL} - V_{SAMP} + V_{EXP}\right) = n_C RT_a + n_E RT_a \tag{D.3}$$

Substituting from equations (D.1) and (D.2) into (D.3)

$$V_{CELL} - V_{SAMP} = \frac{P_a - P_2}{P_2 - P_1} V_{EXP} \tag{D.4}$$

If we rearrange this equation,

$$V_{SAMP} = V_{CELL} - \frac{V_{EXP}}{\frac{(P_1 - P_a)}{(P_2 - P_a)} - 1} \tag{D.5}$$

Since P_1, P_2 and P_a are expressed in equations (D.1) through (D.5) as absolute pressures and equation (D.5) is arranged so that P_a is subtracted from both P_1 and P_2 before use, new P_{1g} and P_{2g} may be redefined as gauge pressures

$$P_{1g} = P_1 - P_a \tag{D.6}$$

$P_{2g} = P_2 - P_a$ (D.7)

And equation (D.5) rewritten as

$$V_{SAMP} = V_{CELL} - \frac{V_{EXP}}{\frac{P_{1g}}{P_{2g}} - 1} \quad \text{(D.8)}$$

This equation (D.8) then becomes the working equation for the Multivolume Pycnometer 1305.

D.2. Sample Calculation

Sample Code AC4.3

V_{CELL}= 7.991 cm^3

V_{EXP}= 6.062 cm^3

V_{SAMP}= 0.583 cm^3

m_{SAMP}= 0.9746 g

$$\rho_{SAMP} = \frac{m_{SAMP}}{V_{SAMP}} = \frac{0,9746}{0,583} = 1,6725 \text{ g/cm}^3$$

APPENDIX E

TABULATED FORM OF CHEMICAL COMPOSITIONS OF ACTIVATED CARBONS

Table E.1 Chemical Compositions of Activated Carbons

Sample Code	C (%)	H (%)	O(%) (by difference)	Ash(%)
AC3.1	73.7	2.8	18.1	5.4
AC3.2	74.8	2.9	18.4	3.9
AC3.3	79.9	2.9	14	3.2
AC3.4	66.2	4.1	25.8	3.9
AC4.1	84.7	2.4	8.3	4.6
AC4.2	84.7	2.4	8.4	4.5
AC4.3	76.5	3.3	14.4	5.8
AC4.4	76.1	3.5	15.2	5.2
AC5.1	75.5	2.9	18.4	3.2
AC5.2	82.9	1.8	7.7	7.6
AC5.3	83.4	1.9	7.2	7.5
AC5.4	74.2	2.9	15.2	7.7

APPENDIX F

TGA FIGURES OF RAW AND IMPREGNATED APRICOT STONES

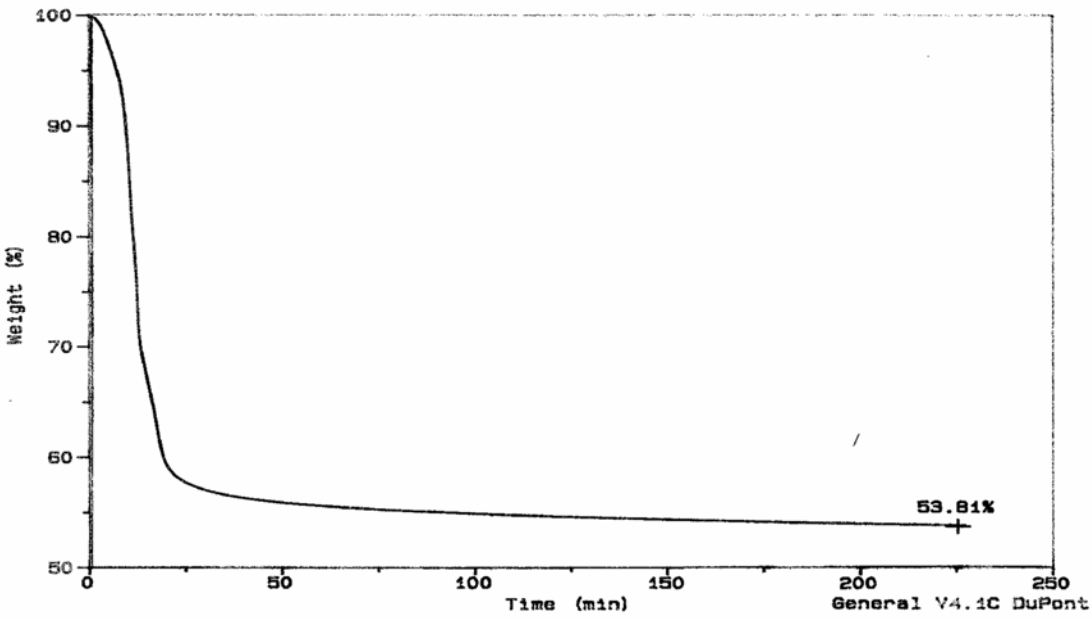

Figure F.1 TGA Result of Acid Impregnated Sample for T=300°C

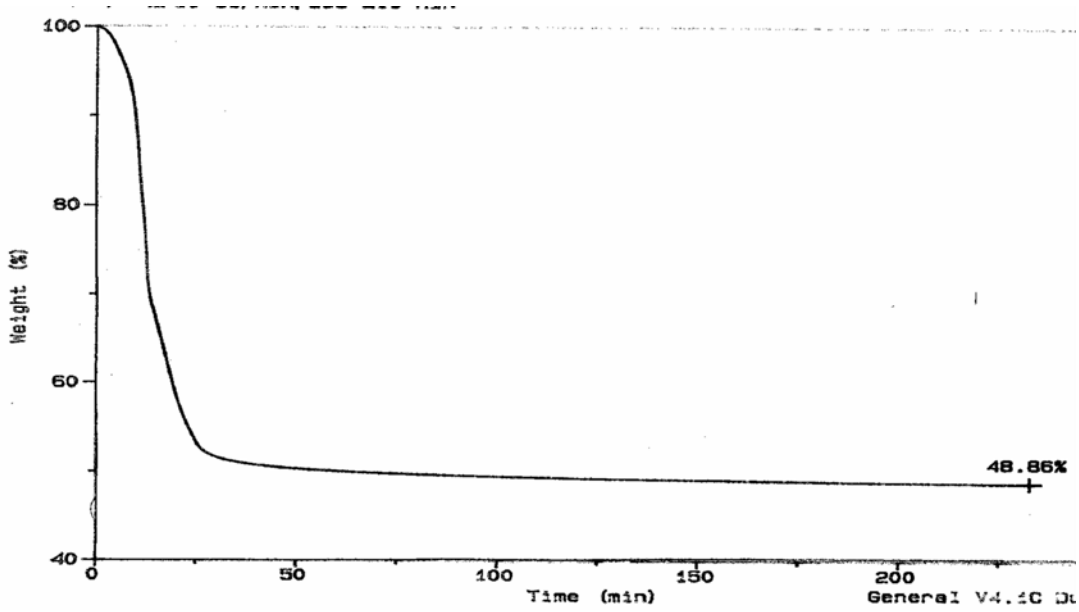

Figure F.2 TGA Result of Acid Impregnated Sample for T=400°C

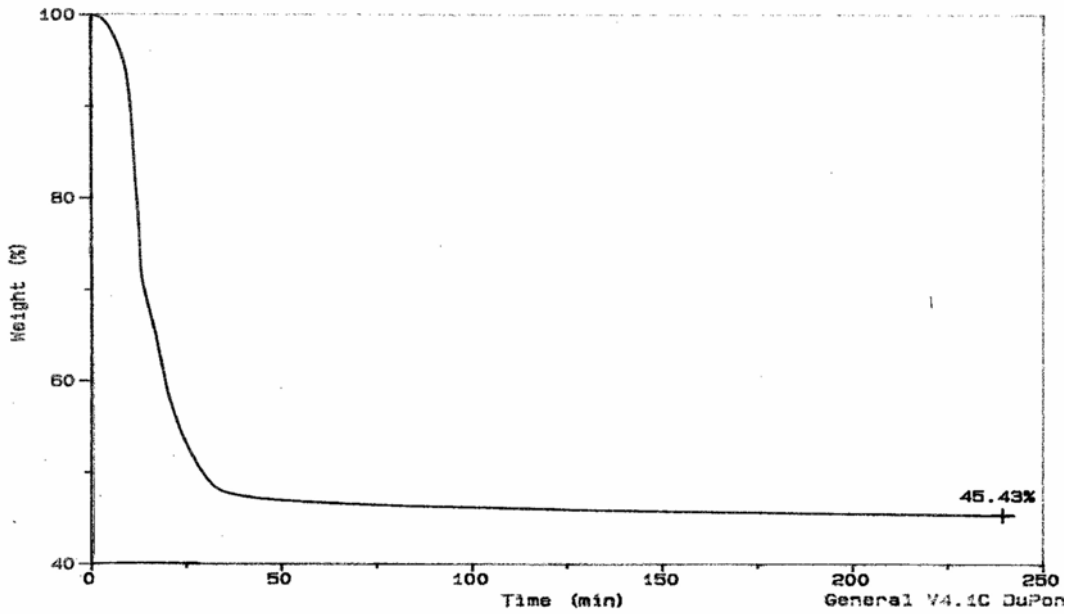

Figure F.3 TGA Result of Acid Impregnated Sample for T=500°C

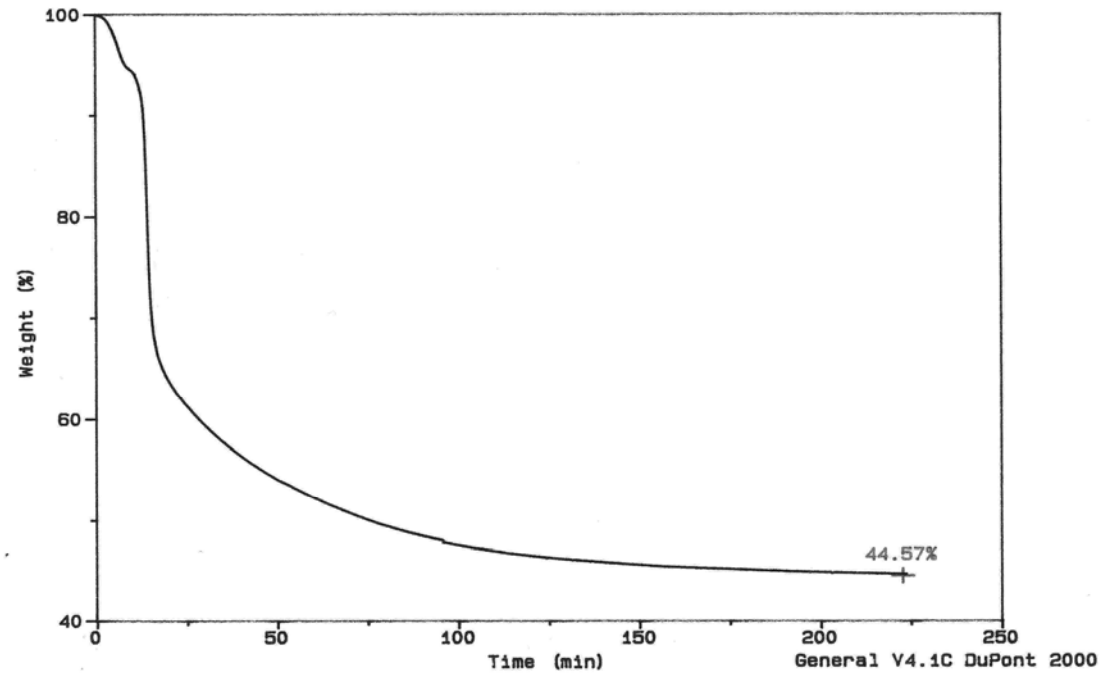

Figure F.4 TGA Result of Raw Apricot Stones Sample for T=300°C

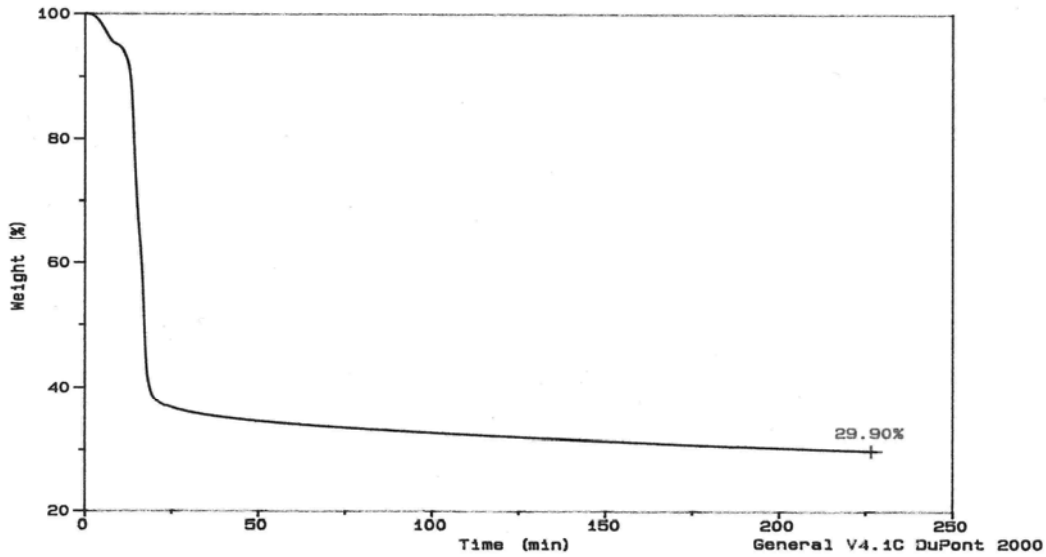

Figure F.5 TGA Result of Raw Apricot Stones Sample for T=400°C

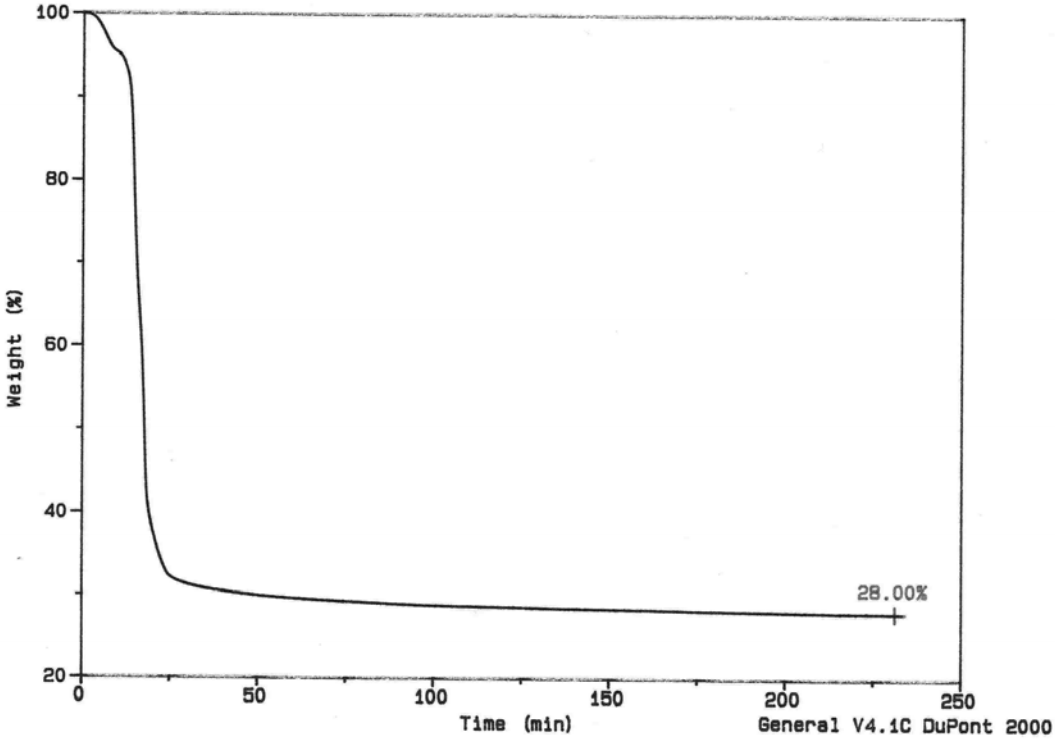

Figure F.6 TGA Result of Raw Apricot Stones Sample for T=500°C